Elsevier Editorial System(tm) for Journal of Catalysis

Manuscript Draft

Manuscript Number:

Title: Ru/Al2O3 catalyzed CO2 hydrogenation: Oxygen-exchange on metal-support interfaces

Article Type: Research paper

Keywords: CO2; Methanation; Reverse water-gas shift; Oxygen exchange; Interface.

Corresponding Author: Dr. Yihu Dai, Ph.D.

Corresponding Author's Institution: Nanjing Tech University

First Author: Yong Yan, Ph.D.

Order of Authors: Yong Yan, Ph.D.; Qiaojuan Wang; Chunyang Jiang; Di Lu; Yihu Dai, Ph.D.; Hongming Wang, Prof.; Yanhui Yang, Prof.

Dear Prof. Liu,

We would like to submit a revised version of our manuscript entitled "Ru/Al_2O_3 catalyzed CO_2 hydrogenation: Oxygen-exchange on metal-support interfaces" (Ms. No. JCAT-17-1516) for your consideration for publication as a research paper in Journal of Catalysis.

In this work, the structure-selectivity relationship and the interfacial oxygen-exchange pathway were presented in γ-Al_2O_3 supported Ru catalyzed CO_2 hydrogenation at atmospheric pressure. Three structural configurations of Ru sites consisting monolayer, periphery and nanocluster were prepared by the control of metallic loadings and carefully characterized. By combining of the experimental and theoretical analyses, it was demonstrated that the monolayer Ru sites energetically preferred the rWGS route while the relatively larger Ru nanoclusters preferred the methanation route. Furthermore, the oxygen-exchange between O atom in gaseous CO_2 and the bridged Ru-O-Al interfaces as well as its catalytic effects in the CO_2 activated dissociation have also been demonstrated by isotope-labeling evidences and calculation results.

The reviewers provided valuable comments and revision advices. As suggested, several experiments have been performed to improve this work. Main improvements in the revised edition are listed below:

(1) The further structural characterizations of Ru catalysts were performed. STEM analyses revealed the difference between 1% and 3% Ru/Al_2O_3.

(2) The catalytic performance under different CO_2:H_2 ratio was examined and the results further verified the diverse Ru sites existed in 1-3% Ru/Al_2O_3 catalysts. The DFT calculation of CO desorption and the experiment of CO hydrogenation reaction were performed to deny the CO-intermediated pathway in CH_4 formation.

(3) The manuscript has been well-reorganized to emphasize the interfacial effects in Ru/Al_2O_3 and the oxygen-exchange process during the CO_2 activation. Several proper references were cited for supporting proposed conclusions and all the figures have been redrawn for the better display.

We are thankful to the referees for their review of the manuscript and for helpful suggestions to improve the quality of our manuscript. Our detailed responses to the comments are listed on the following pages. The invitation letter for resubmission is also attached for your reference.

Thank you for your consideration of our work.

Sincerely yours,

Dr. Yihu Dai
Institute of Advanced Synthesis, School of Chemistry and Molecular Engineering, Jiangsu National Synergetic Innovation Center for Advanced Materials, Nanjing Tech University, Nanjing 211816, P. R. China
E-mail: ias_yhdai@njtech.edu.cn

Prof. Hongming Wang
Institute of Advanced Study, College of Chemistry, Nanchang University, Nanchang 330031, P. R. China
E-mail: hongmingwang@ncu.edu.cn

Prof. Yanhui Yang
Institute of Advanced Synthesis, School of Chemistry and Molecular Engineering, Jiangsu National Synergetic Innovation Center for Advanced Materials, Nanjing Tech University, Nanjing 211816, P. R. China
E-mail: yhyang@njtech.edu.cn

The invitation letter for resubmission

Ref.: Ms. No. JCAT-17-1516

Title: Selective CO_2 hydrogenation activated at the metal-support interfaces

Authors: Yong Yan; Chunyang Jiang; Yao Yao; Yihu Dai, Ph.D.; Hongming Wang; Yanhui Yang

Article Type: Research paper

Dear Dr. Dai,

Thank you for giving us the opportunity to consider your manuscript "Selective CO_2 hydrogenation activated at the metal-support interfaces".

If you can suitably revise the manuscript following the two reviewers' comments, as appended below, I would like to encourage you to resubmit the revised manuscript to the Journal of Catalysis at a later date.

Yours sincerely,

Haichao Liu, Editor

Journal of Catalysis

Email: JCAT@elsevier.com

Elsevier Editorial System: http://ees.elsevier.com/jcat

JCAT Online: http://www.elsevier.com/locate/jcat

http://www.sciencedirect.com/science/journal/00219517

Comment reply

Reviewer #1:

This paper reports an analysis of CO_2 reduction by H_2 over Ru/Al_2O_3 catalysts where Ru weight loading was varied to control active site distributions. In all cases it was observed that CH_4 formation was the preferred pathway, although at lower loadings there was an increase in CO selectivity. Through a series of characterization studies it was argued that CO selectivity trended with particle geometry, where "flat" Ru particles were present in a higher fraction on low loading samples. DFT calculations and isotopic labeling experiments were used to further analyze this phenomenon. While there is a lot of nice analysis in the paper, there are major issues that must be addressed before publication could be recommended. These are described below.

Comment 1: It is stated that CO cannot be an intermediate for CH_4 formation due to a higher barrier for CO formation than CH_4 formation. While it makes sense that CO in the gas phase is not an intermediate for CH_4 formation, CO* (adsorbed CO) can certainly still be an intermediate with CH_4 formation and consistent with the data, if CO desorption is the rate limiting step for RWGS on Ru. The pathways for this reaction on Ru, where CO* was an intermediate for CH_4 and CO, and consistency with previous kinetic measurements was recently reported (see Journal of Catalysis, 2016, 343, 86-96). This work, and reaction pathways including CO* as an intermediate for CH_4 formation, should be considered.

Response: Thank you very much for your kind suggestions. We agree with the possibility that CO* acts as the intermediate for CH_4 formation on Ru/Al_2O_3 catalyst. To resolve the doubt, the energy profiles of CO* desorption in rWGS reaction route on both monolayer Ru_9/Al_2O_3 and cluster Ru_{35}/Al_2O_3 structure models have been calculated, as shown in **Fig. 1**. The energy barrier for CO desorption on both models is relatively low, indicating that the direct desorption of CO* to produce gaseous CO is energetically favored as compared to the consecutive reaction with H* to CH_4. This

also suggests that the CO* desorption can not be the rate-limiting step for rWGS reaction on Ru/Al_2O_3 catalyst.

Furthermore, CO hydrogenation reaction was performed over 1% Ru/Al_2O_3 catalyst to verify whether CO serves the intermediate for the CH_4 formation. The gas feeding ratio of $CO:H_2$ was 1:3 and the same contact time was used in the reaction test. In the reaction temperature range of 150-400 ^oC, no CO conversion was observed and no CH_4 was detected as the product. This experimental result excludes the pathway of CO-intermediated methanation on Ru/Al_2O_3 catalyst.

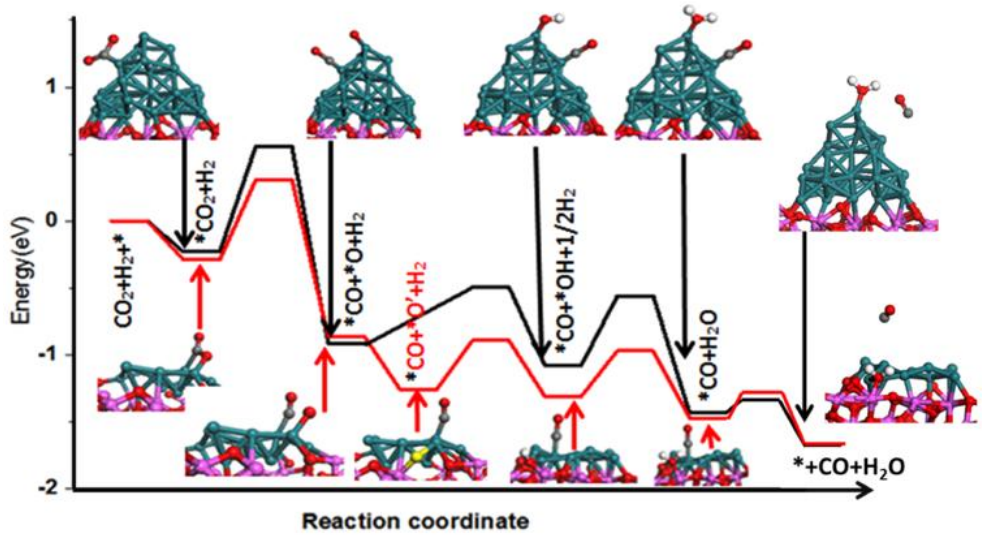

Fig. 1. Energy profiles for rWGS route on Ru_{35}/Al_2O_3 and Ru_9/Al_2O_3 models.

Comment 2: The CO IR data is used to suggest that ~50% of adsorption sites exist as monolayers in the 1% sample, while almost no monolayers exist for the 3% sample. The authors should show whether this is consistent with a linear combination of geometric models of monolayers and particles in the prediction of average coordination number and dispersion. Further, if 50% of Ru is in monolayer structure for the 1% sample, the XAS data should suggest demonstrate a significant scattering contribution of Rh-O bonds (all Ru in monolayers make bonds to support O) and should likely show characteristics of cationic Ru.

Response: Thanks for your valuable comments. The IR spectra of CO adsorption offers a semi-quantitative analysis for the concentration of different surface Ru atoms

in the total exposed Ru sites. It should be noted that the analysis excludes the Ru atoms inside the relatively larger nanoclusters or nanoparticles in which they are the great majority of Ru in the catalysts. Therefore, in consideration of 45% fraction and 30% dispersion for 4 nm Ru NPs, the fraction of monolayer Ru atoms is estimated as ~20% in total Ru atoms of 1% Ru/Al_2O_3 catalyst. In addition, partial Ru atoms in the monolayer sites on the surface with Ru-Al or Ru-Ru bonds, which diminishes the contribution of Ru-O bonds as detected by EXAFS spectra. It has been demonstrated that the chance to detect Ru-O bonds by EXAFS was relatively low even on a catalyst with dispersion of up to 95% (J. Am. Chem. Soc., 137 (2015) 8672). It was also supported by the similar results reported by Ali M. Abdel-Mageed and co-workers, (J. Catal., 335 (2016) 79; ChemSusChem, 8 (2015) 3869). Furthermore, Ru monolayers of 9-13 atoms with the dimension of <1nm have a first Ru-Ru shell CN of 3-5, which has been reported by Karim and co-workers (J. Am. Chem. Soc., 131 (2009) 12230). This can explain a relatively lower CN number of Ru-Ru in 1% Ru/Al_2O_3 as compared to that of 2% and 3% Ru/Al_2O_3 catalysts. Given the above discussion, it is reasonable for the missing signal of Ru-O scattering in EXAFS spectrum of 1% Ru/Al_2O_3 catalyst.

Comment 3: The DFT calculations of activation barriers for single steps should not be compared to the Eapp measured from experiments. If a comparison is to be made it must be done using microkinetic modeling with DFT derived energies corrected for temperature and pressure. Further, the DFT calculations do not consider the CO* desorption step in the RGWS pathway, which most likely will be identified as the RLS for this pathway.

Response: Thanks for your valuable suggestion. The related discussion of comparison of Ea and activation barrier from DFT calculations has been removed from the manuscript. Further, the energy profile of CO* desorption in rWGS reaction route on both monolayer Ru_9/Al_2O_3 and cluster Ru_{35}/Al_2O_3 structure models has been calculated (details are shown in the **response to comment 1** and **Fig. 1**). The energy

barrier for CO desorption on both models is relatively low, indicating that it can not be the rate-limiting step for rWGS reaction on Ru/Al_2O_3 catalyst.

Comment 4: The isotopic labeling experiments do not consider the well known ability of metal supported on Al_2O_3 to drive CO_2 scrambling with fast kinetics. See work of Duprez or for example (Langmuir, 2003, 19 (21), pp 8793-8800).

Response: Thanks for your valuable suggestion. As previous works demonstrated, the exchange of O species between surface carbonates and oxides substance can rapidly occur on the metal oxide surface under the pure CO_2 atmosphere. In our case, however, the mixture gas-feeding of H_2 and CO_2 diluted in He was used, which might greatly alter the kinetic behaviors of oxygen-exchange over Ru/Al_2O_3 catalyst. In addition, to exclude the possibility of CO_2 scrambling with fast kinetics, pure $C^{18}O_2$ has been pre-fed for a sufficient time to reach equilibrium before the introduction of H_2 to start the reaction. In this work, a second run was performed and the ^{18}O-labed catalyst was also used to independently verify the exchange pathway.

Reviewer #2:

General comment: The authors investigated the reaction mechanism of CO_2 hydrogenation over Ru/Al_2O_3 catalysts. In particular, they focused on the Ru shape effect on the reaction. They concluded that CO_2 is converted to CO on monolayer Ru, while CO_2 is methanated on 3D Ru clusters. However, I wonder why they chose Ru/Al_2O_3 catalysts for this study because of their low activity in CO_2 hydrogenation (J. Catal. 129 (1991) 130, React. Kinet. Catal. Lett. 71 (2000) 55). In addition, the authors should show the difference from the reported paper in ACS Catal. (ACS Catal. 3 (2013) 2449).

Response: Thank you very much for your valuable comments. Kawk et al. have presented nice works on the relationship of particle size and catalytic selectivity in the CO_2 hydrogenation reaction over Ru/Al_2O_3. In this work, we chose widely-studied Ru/Al_2O_3 as the model catalyst and similar experimental observation was also obtained. We performed isotope-labeling characterizations and theoretical

calculations to further reveal the metal-support interfacial effects in the CO_2 activation step. Especially, the oxygen-exchange between O in CO_2 and bridged Ru-O-Al interface with a relatively lower energy barrier was observed during Ru/Al_2O_3 catalyzed CO_2 activation. We believe the exchange process might be general for the CO_2 activation mechanisms over Ru supported on different oxides, and we are extending the catalyst system of supported Ru. The findings in this work would be helpful for the design of efficient catalyst based on the deep understanding of the mechanism.

Specific comment 1: Furthermore, the meaning of the kinetic results is unclear. When the authors try to clarify that CO and CH_4 are formed in parallel, the authors should show the effect of space velocity on the reaction. I cannot understand that only Ea results predicted "CO and CH_4 were formed either by different route and/or different active sites" (page 10). If CO_2 hydrogenation is a stepwise reaction of RWGS and CO methanation, the real CO reaction rate should be the sum of the CO and CH_4 reaction rate which the authors estimated in Fig. 1. At the present stage, the authors did not discuss the mechanism consisting of the stepwise reaction. When the Arrhenius plots are shown, moreover, the authors should give the low conversion of a reactant (< 10%). This is a declaration that the authors assumed a differential reactor.

Response: Thanks for your comments. We have been reorganized the manuscript to deduce the conclusion that the different Ru active sites exist in the Ru/Al_2O_3 with 1-3 wt% Ru loadings and determine the diverse catalytic activity and selectivity in CO_2 hydrogenation reaction. The temperature-dependence performance and the Arrhenius plots revealed that 1% and 3% Ru/Al_2O_3 catalysts had different preference for either rWGS or methanation route. The reaction rates under different CO_2:H_2 ratio and similar TOF of total CO_2 conversion were further examined and the different variation trends of TOF for CO and CH_4 formation suggested that the distinct Ru active sites are existed in 1% and 3% Ru/Al_2O_3 catalysts (**Fig. 1**).

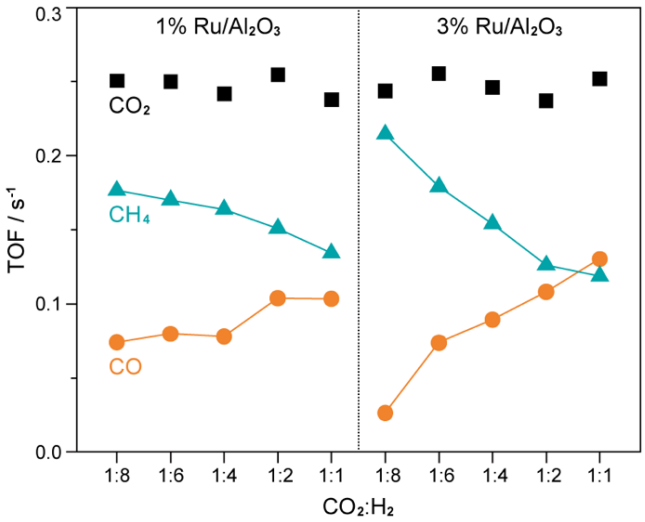

Fig. 1. The TOF for conversion of CO_2, production of CO and CH_4 over 1% and 3% Ru/Al_2O_3 catalysts as a function of CO_2:H_2 ratio.

It is indeed possible that CH_4 formation occurred via CO intermediation on Ru/Al_2O_3 catalyst. However, the DFT calculation of CO* desorption on both monolayer Ru_9/Al_2O_3 and cluster Ru_{35}/Al_2O_3 structural models demonstrated that the step could easily accomplish with relatively lower energy barriers (**Fig. 2**). This indicated that the direct desorption of CO* to produce gaseous CO is energetically favored as compared to the consecutive reaction with H* to CH_4. This also suggested that the CO* desorption can not be the rate-limiting step for rWGS reaction on Ru/Al_2O_3 catalyst.

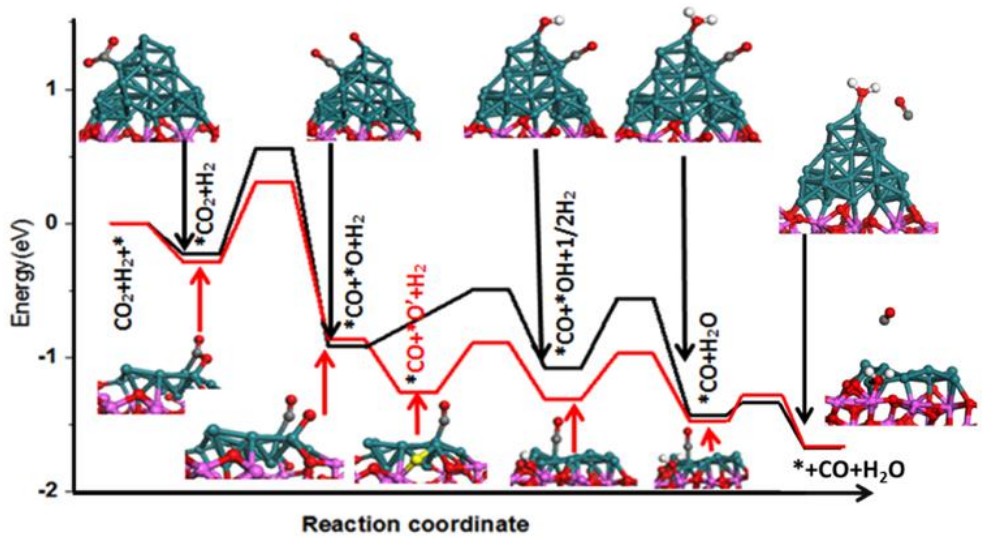

Fig. 2. Energy profiles for rWGS route on Ru_{35}/Al_2O_3 and Ru_9/Al_2O_3 models.

Furthermore, CO hydrogenation reaction was performed over 1% Ru/Al_2O_3 catalyst to verify whether CO serves the intermediate for the CH_4 formation. The gas feeding ratio of $CO:H_2$ was 1:3 and the same contact time was used in the reaction test. In the reaction temperature range of 150-400 ^oC, no CO conversion was observed and no CH_4 was detected as the product. This experimental result excludes the pathway of CO-intermediated methanation on Ru/Al_2O_3 catalyst.

In the end, we would like to confirm the experimental details that the low conversion of CO_2 (<15%) was achieved for each Arrhenius plot. We have added the related explanation in the section of **3.1 Catalytic performances and kinetics** in the revised manuscript.

Specific comment 2: Based on the XAS and HR-TEM, I cannot find any difference of Ru shape between the prepared catalysts. The authors calculated the CN of Ru particles. In my opinion, its significant figure is one digit, so 6.51 of CN is same to 7.29-7.43 of CN. Although the only evidence of the monolayer formation seems appearance of FTIR peaks at 2130 and 2072 cm^{-1}, there is a possibility that those peaks can be attributed to CO on cationic Ru (Catal. Lett. 51 (1998) 41, Chem. Select. 1 (2016) 3197). Thus, the authors must deny the presence of the cationic Ru.

Response: Thanks for your useful advices. The diverse structural sites including monolayer, periphery and nanocluster were observed to be co-existed in each Ru/Al_2O_3 catalyst, which is supported by the FTIR spectra of CO adsorption. However, the distributions of individual Ru site are distinctly different for 1-3 wt% Ru/Al_2O_3 catalysts. For instance, the STEM analyses revealed the difference. The disappearance of Ru nanoparticles was observed in the most investigation area for 1% Ru/Al_2O_3 catalyst. However, it is so intuitive for 3% Ru/Al_2O_3 catalyst that small Ru nanoparticles dispersed on the Al_2O_3 supports individually (**Fig. 3**).

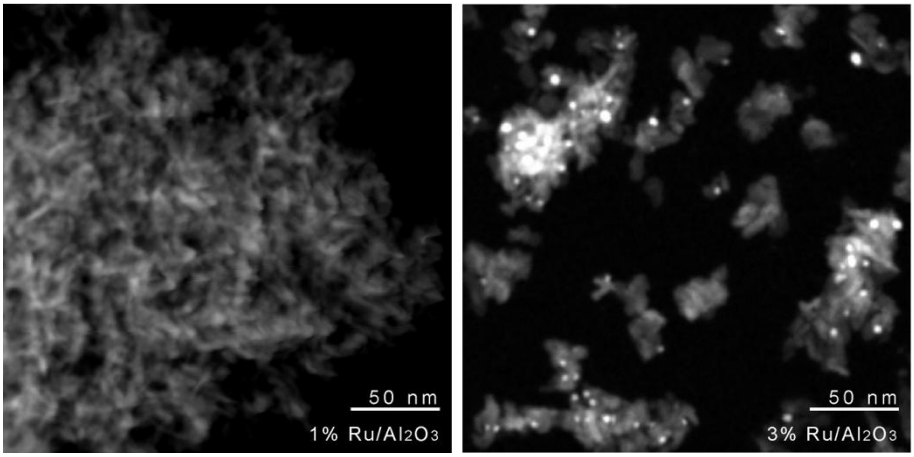

Fig. 3. STEM images of 1% and 3% Ru/Al_2O_3 catalysts.

All Ru/Al_2O_3 catalysts were pretreated with 500 ^oC reduction in 10% H_2/He to avoid the oxidation of Ru species into RuO_2. However, the existence of periphery Ru atoms leads to the partial oxidation of Ru. The direct bond of monolayer Ru atoms to the Al_2O_3 support also causes the oxidative status of Ru. In addition, such oxidative $Ru_n^{\delta+}$ species are not easily reduced and thus alter the activation behaviors of CO_2 as well as the adsorption of CO which was identified by the IRAS spectra.

Specific comment 3: It is challenging to conclude that CO_2 is methanated on the top sites of 3D Ru clucters (page 20 and Scheme 1). According to the hypothesis, the activity in CO_2 methanation would not depend on the support nature, while the fact is different (J. Catal. 129 (1991) 130, React. Kinet. Catal. Lett. 71 (2000) 55).

Response: We understand the concerns. The competitive coexistence of rWGS and methanation reactions over Ru/Al_2O_3 catalyst with multiple Ru sites may not conclude that CO_2 is methanated only on the top sites of 3D Ru clucters or CO is formed completely on the monolayer Ru sites. In consideration of small gaps for the Ea values of rWGS and methanation route, it is evidenced that the individual Ru site had a preference but not a 100% hydrogenation selectivity. For instance, 3D Ru cluster sites favor the methanation, which is consistent with many previous reports. However, the effect of supports can not be ignored. The support not only affected the structure of Ru as a result of the metal-support interaction but also impacted on the

particle size due to the difference in pore structures and BET surface area (J. Catal., 92 (1985) 296). Besides, the surface properties of supports, such as basicity/acidity, determined the activation behavior of the reactants, including the adsorption of CO_2 (J. Chem. Soc. Faraday Trans., 77 (1981) 1003.). The concentrated surface CO_2 was beneficial for the following activation by Ru to be hydrogenated into CH_4, which was attributed to the 'adsorption enhanced' activation.

***Referee Suggestions**

We would like to suggest the following potential reviewers:

(1) Prof. Jingguang Chen

Chemistry Division, Brookhaven National Laboratory, Upton, NY 11973, USA.

Department of Chemical Engineering, Columbia University, New York, NY 10027, USA.

E-mail: jc3972@columbia.edu

(2) Prof. Ding Ma

College of Chemistry and Molecular Engineering, Peking University Beijing 100871, China

E-mail: dma@pku.edu.cn

(3) Prof. Emiel J. M. Hensen

Department of Chemical Engineering and Chemistry

Eindhoven University of Technology, 5600 MB Eindhoven, Netherlands

E-mail: e.j.m.hensen@TUE.NL

(4) Prof. Jinlong Gong

Key Laboratory for Green Chemical Technology of Ministry of Education, School of Chemical Engineering and Technology, Tianjin University, Tianjin 300072, China

E-mail: jlgong@tju.edu.cn

Ru/Al_2O_3 catalyzed CO_2 hydrogenation: Oxygen-exchange on metal-support interfaces

Yong Yan[a,b], Qiaojuan Wang[a], Chunyang Jiang[a], Di Lu[a], Yihu Dai[a,*], Hongming Wang[c,*], Yanhui Yang[a,*]

[a]Institute of Advanced Synthesis, School of Chemistry and Molecular Engineering, Jiangsu National Synergetic Innovation Center for Advanced Materials, Nanjing Tech University, Nanjing 211816, China

[b]School of Chemical and Biomedical Engineering, Nanyang Technological University, Singapore 637459, Singapore

[c]Institute for Advanced Study and Department of Chemistry, Nanchang University, Xuefu Dadao 999, Nanchang 330031, China

Corresponding authors:

*E-mail: ias_yhdai@njtech.edu.cn (Dr. Y. H. Dai)

*E-mail: hongmingwang@ncu.edu.cn (Prof. H. M. Wang)

*E-mail: yhyang@njtech.edu.cn (Prof. Y. H. Yang)

Abstract

The metal-support interfaces of metallic nanoparticles supported on oxide determine the activated dissociation of CO_2 in CO_2 hydrogenation. It also guides the catalytic pathway towards either CO_2 methanation or reverse water-gas shift (rWGS). In this work, Ru/Al_2O_3 catalysts with different Ru structural configurations were prepared by controlling the Ru weight loadings, which revealed the structure-dependence of production rates for CO and CH_4 formation with different apparent activation energies. Based on the characterization results, two catalyst models were setup: the Ru_9/Al_2O_3 model consisted an interface of monolayer Ru sites tightly contacted with γ-Al_2O_3 supports, and the Ru_{35}/Al_2O_3 model represented a relatively larger Ru nanocluster supported on γ-Al_2O_3. Theoretical calculations of these two models demonstrated that monolayer Ru sites favored the rWGS route with a relatively low energy barrier for both CO_2 activation and CO formation steps, while Ru nanoclusters preferred methanation route energetically. Furthermore, the combination of theoretical calculations and experimental isotope-exchange measurements suggested that the interfacial O species in Ru-O-Al interfaces acted a critical role in CO_2 activation via oxygen-exchanging with the O atom in the feeding CO_2 and consequently incorporating into the final hydrogenation product.

Keywords: CO_2, methanation, reverse water-gas shift, oxygen exchange, interface

1. Introduction

The catalytic conversion of CO_2 to useful products such as CO or carbon-neutral fuels is an essential reaction process since it involves carbon recycle with fundamental research interest and potential industrial applications as well as the environmental implications [1,2]. In consideration of the thermodynamic stability of CO_2 and the high energy barrier for splitting C=O bond, the effective CO_2 activation deems as a critical step in improving the kinetics for overall reaction. Undoubtedly, it needs the rational design of the promising heterogeneous catalysts based on the mechanistic understandings of CO_2 activation and reaction pathway [3-5].

The hydrogenation of CO_2 at atmospheric pressure is of great significance for CO_2 utilization, which proceeds via either reverse water-gas shift (rWGS) to yield CO or methanation reaction to produce CH_4 [6,7]. Although the processes have been thoroughly studied from the beginning of the 20th century [8], no consensus has been reached for the activation mechanism. A bi-functional mechanism was verified on supported Pd catalysts in which H_2 dissociation on metallic Pd particles and CO_2 activated adsorption on metal oxide support occurred synergistically to produce CH_4 via the formation of carbonates intermediates [9]. As a comparison, the Pd/SiO_2 catalyst without effectively active oxides almost exclusively yielded CO in the CO_2 hydrogenation reaction [10,11]. This concept was further validated by the inactive performance of Pd supported on inert multi-walled carbon nanotubes [12]. In addition, another mechanism of the direct activated dissociation of CO_2 over the metal particles

has been proposed for Ru and Rh catalysts [13-17], which was experimentally observed by both in-situ diffuse reflectance infrared Fourier transform spectroscopy (DRIFTs) and ambient-pressure X-ray photoelectron spectroscopy (XPS) [14,15], and theoretically validated by density function theory (DFT) calculations [16]. Interestingly, both the oxygen vacancy on the support and the metallic Ru particles can serve as the activation sites for CO_2 to form CH_4 over Ru/CeO_2 but via two different reaction pathways [18].

The interface of supported catalyst possesses dual sites of the metal-oxide heterojunction, playing pivotal roles in governing the electronic and chemical structures of the catalysts and the surface reaction process [19-21]. A number of structural factors in the supported metal sites, including the particle size, bimetallic alloying, crystal planes, redox ability and acidity, can finely tune the interfacial effects in the catalytic reactions [22-26]. For instance, smaller nanoclusters gain the characters varying with multiple neighboring sites with versatile geometric and electronic structures, as compared to larger nanoparticles [27]. The acceleration of CO_2 dissociation process at the metal-support interface was observed on the supported catalysts with the optimized metal particle size [28,29]. On the other hand, the support-induced interfacial effects can also allow the tailoring of the electronic structure, the chemical state and the stability of the metal species for the enhancement in the catalytic performance [30]. In hydrogenation chemistry, both the strong metal-support interaction (SMSI) and hydrogen spillover would be subjected to the

interfacial effects [31-34]. The CeO_2 supported metallic Ir nanoparticles select for CH_4 production, while the partially oxidized IrO_x sites that are modulated by a SMSI effect prefer selective production of CO in the hydrogenation of CO_2 [35]. Beaumont et al. have reported that a long-distance hydrogen spillover from Pt to Co sites led the reduction of Co NPs, generating more active sites and therefore dramatically increasing in CH_4 production [36]. By combining experimental characterizations and theoretical calculations, the proper metal-oxide interfaces have been demonstrated to selectively strengthen the binding of C,O-bound and O-bound species, leading to the diverse product selectivity in the CO_2 hydrogenation reaction [37].

Herein, the structure-selectivity relationship and the interfacial oxygen-exchange pathway were presented in γ-Al_2O_3 supported Ru catalyzed CO_2 hydrogenation at atmospheric pressure. Three structural configurations of Ru sites consisting monolayer, periphery and nanocluster were prepared by the control of metallic loadings and carefully characterized. By combining experimental and theoretical analyses, the monolayer Ru sites energetically prefer the rWGS route while the relatively larger Ru nanoclusters prefer the methanation route. Furthermore, the oxygen-exchange between O atom in gaseous CO_2 and the bridged Ru-O-Al interfaces as well as its catalytic effects in the CO_2 activated dissociation have also been demonstrated by isotope-labeling evidences and calculation results.

2. Experimental

2.1 Catalyst preparation

Ru/Al_2O_3 catalysts with metal loadings of 1, 2 and 3 wt% were prepared on commercial γ-Al_2O_3 supports by the incipient wetness impregnation method. Typically, a certain amount of ruthenium (III) acetylacetonate (Sigma-Aldrich) was dissolved in ethanol with the volume decided by the pore volume of the support acquired by nitrogen adsorption-desorption isotherms at -198 °C on a Quantachrome AUTO-SORB-6B static volumetric instrument (~0.8 cm^3/g). The obtained solution was then added dropwise onto the support under intensive mixing. The resulted powder was dried for 12 h at 80 °C and the catalysts were then obtained via calcination at 500 ^oC for 2 h under 10% H_2/He with a flow rate of 100 mL/min.

2.2 Catalyst characterizations

H_2-O_2 titration was carried out on a Micromeritics Autochem II 2920 instrument equipped with a TCD detector to measure the amount of surface metal sites. Typically, 100 mg of catalysts were loaded into a U-tube reactor for analysis. All samples were pretreated in H_2 flow for 60 min at 500 ^oC and then purged with Ar for 30 min before cooling to 30 ^oC in the same atmosphere. A gas flow of 10% O_2/Ar was passed over the samples for 30 min to allow the complete coverage of formed O species on the metal surfaces. After switching the feeding gas to pure Ar, sample was heated up to 250 ^oC and held there until the signal was stable. Subsequently, consecutive pulses of 10% H_2/Ar were dosed at 5 min intervals to consume all the surface oxygen. The exposed Ru surface sites was calculated with the assumed stoichiometry of H_2/Ru = 5/2 [38].

Scanning transmission electron microscopy (STEM) analysis was carried out on a FEI Tecnai G2 F20 S-TWIN system operated at 200 kV. The adsorption of CO accompanied by infrared reflection absorption spectroscopy (IRAS) at 25 ^{o}C was performed on a FTIR spectrometer (Nicolet iS50) equipped with a smart collector and a MCT/A detector cooled by liquid nitrogen. Prior to each experiment, the sample was pretreated at 500 ^{o}C for 60 min in 10% H_2/He and then cooled down in He flow to 25 ^{o}C. The background spectrum was collected after 60 min in He purge, followed by introducing 10% CO/He flow to start the chemisorption. After 30 min in CO/He, the sample was purged in He for another 30 min and the resulted spectrum was then acquired. All spectra were recorded by accumulating 100 scans with a resolution of 4 cm^{-1}.

2.3 Kinetic measurements

For kinetic measurements, a desired amount of catalysts was loaded into a fix-bed quartz tube micro-reactor, which was in-situ reduced in a 10% H_2/He gas flow of 100 mL/min at 500 ^{o}C for 60 min, and then kept at a reaction temperature to measure the activity. The measurements were carried out at atmospheric pressure by passing a gaseous mixture of CO_2 (5%) and H_2 (20%) in He balance at a total flow rate of 100 mL/min. The inlet and outlet flows were analyzed by an on-line gas chromatograph (Agilent 6890) equipped with both a FID and a TCD detector. The sampling data were collected when reaction reached a steady state (~60 min after

reaching the desired reaction temperature). The kinetic measurement was performed by keeping the CO_2 conversion below 15%.

2.4 First-principles calculations

Density functional theory (DFT) calculations were carried out to investigate the catalytic reaction mechanism of CO_2 hydrogenation on Al_2O_3-supported Ru clusters. The Al_2O_3-supported Ru_{35} cluster and single layer Ru_9 cluster were constructed by binding the Ru_{35} and single layer Ru_9 cluster onto a γ-Al_2O_3(100) surface. The unit cell of the amorphous Al_2O_3 surface for periodic DFT calculation has a dimension of 10 × 13 × 18 Å, with a vacuum space of 15 Å. All the calculations were carried out using the GGA functional with a projector-augmented wave basis set implemented in the Vienna Ab initio Simulation Package [39-41]. The energy cutoff of 350 eV was used. For the Al_2O_3 supported catalyst, atoms in the top two layers of the Al_2O_3 slab and adsorbed species were allowed to relax while the bottom layers of the Al_2O_3 slab were kept static.

2.5 Isotope-exchange experiments

For the isotope-exchange experiments, the as-calcined catalyst was loaded into a fixed bed quartz reactor, followed by reducing at 500 ° C for 60 min under 10% H_2 /He (flow rate=50 mL/min). Pure He or different mixtures, 1% $C^{18}O_2$ (95%-^{18}O, Linde North America Inc.) or $C^{16}O_2$, and/or 4% H_2 diluted in He, were switched and introduced into the reactor. The gases at the outlet of the reactor were analyzed by a mass spectrometer (GAM 300, InProcess Instruments) by following the evolution of

the m/z=48 ($C^{18}O_2$), 15 (CH_4), 20 ($H_2{}^{18}O$), 18 & 17 ($H_2{}^{16}O$), 30 ($C^{18}O$), 28 ($C^{16}O$) with the response time of the mass spectrometer following a change in gas concentration being less than 2 s.

3. Results and discussion

3.1 Catalytic performances and kinetics

There was a hypothesis that the conversion of CO_2-to-CO could be completed via the consequent reaction processes, the formation of surface carbonates from CO_2 adsorption and the release of gaseous CO from the direct interaction between formed carbonates and the surface oxygen species in the metal oxide support [42]. Therefore, the catalytic effects of bare γ-Al_2O_3 support in the CO_2 reduction reaction became one of the first concerns. The reference test was carried out under identical reaction conditions and neither CO nor CH_4 was detected as the product over γ-Al_2O_3 support. The involvement of Ru sites with/without interaction with Al_2O_3 support was essential in the reaction.

Fig. 1 showed dependences of the catalytic performance on reaction temperature in the CO_2 hydrogenation over Ru/Al_2O_3 catalysts with three Ru loadings. Two reaction pathways, CO_2 methanation to form CH_4 and reverse water-gas shift (rWGS) reaction to form CO, competitively occurred in the reaction on these catalysts. The CO_2 conversion curves were presented in Fig. 1A. 3% Ru/Al_2O_3 catalyst showed the superior CO_2 conversion with the onset temperature at approximately 200 ^oC and the maximum conversion of 80% at 400 ^oC. Further increasing reaction temperature led

to the decline in CO_2 conversion due to the thermodynamic equilibrium limitation. Similar curves of CO_2 conversion were obtained on 2% and 1% Ru/Al_2O_3 catalysts, however, higher onset temperatures and lower maximum activities displayed.

With increasing the reaction temperature, the identical variation trend of CH_4 yield with the weight loading of Ru was observed, compared with that of the CO_2 conversion. However, it was a contrary dependency of CO yield (selectivity) with the weight loading of Ru. As shown in Fig. 1B, the formation of CO started at approximately 300 ^oC and increased with ramping temperatures, and the CO yield was the highest over 1% Ru/Al_2O_3 of being 17.4% at 450 ^oC, which was twice of that over 3% Ru/Al_2O_3 catalyst, indicating that CH_4 formation was favored and CO formation was suppressed with increasing Ru loadings.

To measure the specific reaction rates and the apparent activation energies (E_a) of three Ru/Al_2O_3 catalysts in a certain temperature window, less than 15% CO_2 conversions were achieved by regulating the usage amount of the catalysts. The Arrhenius plots for CH_4 and CO formation were separately displayed in Fig. 2A and Fig. 2B. For 3% and 2% Ru/Al_2O_3 catalysts, the E_a value for CH_4 formation was 65.0±3.5 kJ/mol (0.67±0.04 eV) while that for CO formation was 75.0±4.3 kJ/mol (0.78±0.04 eV). The distinctly different E_a values have been observed on 1% Ru/Al_2O_3 catalyst, which the calculated E_a for CH_4 formation increased to 73.6±3.2 kJ/mol (0.76±0.03 eV), and the E_a for CO formation decreased to 67.1±2.7 kJ/mol (0.69±0.03 eV). Comparable results have been reported that E_a of 67.4 and 72.0

kJ/mol were obtained on Ru/Al_2O_3 and Ru/SiO_2 catalysts, respectively [43-45]. There was also an experimental observation that the E_a for CH_4 and CO formation varied with different metal loadings for Pd/Al_2O_3 and Rh/Al_2O_3 catalysts, due to the particle size effects and the different roles of individual active sites [46]. In this study, the different E_a values strongly supported the opposite preference of the production of CO or CH_4 on Ru/Al_2O_3 catalysts with different Ru loadings. It could be expected that different reaction routes proceeded on different active sites during the CO_2 reduction reaction.

The Ru site-specific TOF for CH_4 and CO production was also independently examined over three Ru/Al_2O_3 catalysts under varying CO_2:H_2 ratios and similar level of TOF_{CO2} (approximately 0.25 s^{-1} for total CO_2 conversion) (Fig. 3). When the ratio of CO_2:H_2 was less than the stoichiometric ratio for methanation reaction (1:4), the TOF toward CO formation over 1% $Ru/A_{l2}O_3$ remained constant (~0.08 s^{-1}). As the CO_2:H_2 ratio was increased to more CO_2-rich condition, the TOF of CO formation slightly increased due to the fact that the thermodynamic equilibrium preferred the production of CO rather than CH_4 under the relatively higher CO_2:H_2 ratios. However, for 3% Ru/Al_2O_3 catalyst, the TOF of CO formation increased in direct proportion to the CO_2:H_2 ratio in the full range. The different relationship between the CO production TOF and the CO_2:H_2 ratio was revealed on 1% and 3% Ru/Al_2O_3 catalysts. This result suggested that different types of active Ru sites existed in the two catalysts and the rWGS reaction over Ru catalysts was structure-sensitive process. The

structure-activity relationships in CO_2 reduction reaction catalyzed by Ru/Al_2O_3 with different Ru loadings were further discussed as below.

3.2 Characterizations of Ru surface structures

The dispersions of Ru atoms on catalyst surface were determined from volumetric H_2-O_2 titration measurements via reduction of O_2-precovered Ru surface by 10% H_2/Ar gas at 250 ^oC [38]. The total uptake of H_2 reflected the concentrations of surface Ru sites, which were 2.63×10^{19}, 4.14×10^{19} and 5.71×10^{19} g^{-1} for 1%, 2% and 3% Ru/Al_2O_3 catalysts, respectively. Accordingly, the calculated dispersion of Ru metals decreased with the increase of the Ru weight loading from 1% to 3% (44.5% to 32.2%), as shown in Table 1. As shown in Fig. 4, XRD patterns of three Ru/Al_2O_3 catalysts showed only the diffraction peaks of the γ-phase of commercial Al_2O_3 support. The diffraction peaks corresponding to the metallic Ru^0 and RuO_x species were not discerned, possibly due to the high dispersion of small Ru nanoclusters on γ-Al_2O_3 at low weight loadings.

Fig. 5 showed the k^3-weighted $\chi(k)$ functions (where k was wave number) and corresponding Fourier transforms of EXAFS spectra, providing highly responsive structure information of the local coordination environment of Ru atoms. The bi-shell fitting of Ru-Ru and Ru-O paths can be first ruled out, whereas the single Ru-Ru scattering shell can fit with the measured spectra reasonably, with the resulted structural parameters being presented in Table 1. An increase of CN from 6.51 to 7.29 was observed when Ru loading was changed from 1% to 2%, while the further

increase of Ru loading to 3% only resulted in a marginal increase of the CN to 7.43. The appreciable variation in CN values suggested that there was a prominent structural change for the supported Ru particles from 1% to 2% (3%) Ru/Al_2O_3 catalysts. A correlation between the Ru-Ru first shell CN and the average diameter of Ru particles with *hcp* hemispheric model was reported [44,45]. The increasing CN from 6.51 to 7.43 was corresponding to an increase of the Ru particle size, which equaled to 0.94, 1.27 and 1.32 nm for 1%, 2% and 3% Ru/Al_2O_3 catalysts, respectively. Correspondingly, the dispersions of surface Ru atoms were estimated based on the diameters and the hemispheric structure model, which were 71.6%, 52.7% and 50.8% for 1%, 2% and 3% Ru/Al_2O_3 catalysts, respectively. In contrasted to the results of H_2-O_2 titration that the Ru dispersions of three catalysts are 44.5%, 35.1% and 32.2%, respectively, the values in the range from 50.8% to 71.6% were apparently overestimated, suggesting that the Ru particles in three Ru/Al_2O_3 catalysts did not fully accord with the regular hemispheric structure model. The different structure types may be included for the Ru sites on the γ-Al_2O_3 surface.

The infrared reflection absorption spectroscopy (IRAS) of the chemisorption of CO as the probe molecule on three Ru/Al_2O_3 catalysts was used for providing sensitive structural information of surface Ru sites [47-49]. The IRAS tests were performed at 25 ^{o}C and the spectra were presented in Fig. 6A. Two distinct peaks at high frequencies (HF) of 2130 and 2072 cm^{-1}, along with one at low frequencies (LF) between 2000 and 2050 cm^{-1} were observed over all catalysts. For a better

comparison, the spectra were displayed in Kubelka-Munk (KM) unit and normalized with the peak area at 2130 cm^{-1}.

The LF peak was assigned to the linear CO* ("*" represents the adsorbed species) on top sites of relatively larger three-dimension (3D) Ru nanoclusters that interacted with all surrounding sites by Ru-Ru bonds [50,51]. The blue shift of this peak was caused by the dipole-dipole coupling effect of the adsorbed CO* species with increasing concentrations [52,53]. The two HF peaks at 2130 and 2072 cm^{-1} were associated with CO adsorbed on Ru sites that were perturbed by bonds from the support [53,54]. The peak at 2130 cm^{-1} was ascribed to the symmetric stretches of bi-carbonyl species that adsorbed on the uncoordinated Ru sites at the periphery interface, while the peak at 2072 cm^{-1} was contributed from both the asymmetric stretches of bi-carbonyl species and the vibration of linear adsorbed CO on Ru sites of monolayers [51,53-56]. Therefore, 3D nanoclusters, periphery interface sites and monolayer sites of Ru species were co-existed in Ru/Al_2O_3 catalyst structures. It has also confirmed that ideal hemispheric structure model cannot match with Ru sites in this catalyst system.

A clearly opposite variation tendency of peak intensity for 2070 cm^{-1} peak and LF peak was observed with increasing Ru loadings. To further quantify the surface structural compositions, the IRAS spectra were deconvoluted into Gaussian sub-bands using the coefficient values acquired by Yokomizo et al. [54], as shown in Fig. 6B. Based on the above assignments and analysis method, the distributions of linear

adsorbed CO and bicarbonyls were obtained and the fractions of corresponding Ru sites were listed in Table 1. For three Ru catalysts, the periphery sites of Ru maintained similar proportions. However, the fraction of Ru sites in monolayers has drastically decreased from 45.4% to 6.8% when Ru loading raised from 1% to 2%, while that fraction in 3% Ru/Al_2O_3 was only 1.1%. Conversely, the fraction of top sites in 3D Ru nanoclusters has almost doubled when Ru loading increased from 1% to 2%, while further increasing Ru loading to 3% only resulted in a relatively small increase in the fraction. For 1% Ru/Al_2O_3, both monolayers and 3D nanoclusters with multiple layers were present in an appreciable percentage. For 2% and 3% Ru/Al_2O_3, 3D multilayers dominated the Ru sites. It has been reported that the calcination treatment most likely led to planar Ru sites lying on the γ-Al_2O_3 surface [57]. The HAADF-STEM analyses (Fig. 7) revealed such tendency on 1% Ru/Al_2O_3 catalyst. No formation of Ru nanoparticles was observed in the most investigation area. However, for 3% Ru/Al_2O_3 catalyst, it was so intuitive that small Ru nanoparticles dispersed on the Al_2O_3 support individually.

3.3 Structure-activity relationship

The evolution of the surface intermediate species was monitored by in-situ DRIFT spectra during the CO_2 hydrogenation reaction over 1 wt% Ru/Al_2O_3 catalyst (Fig. 8). The reaction was carried out at 350 ^oC and the equilibrium time was lasted for 90 min under reaction flow of CO_2 and H_2. A clear band at 2000 cm^{-1} was observed, which was ascribed to CO* species serving as the intermediate for rWGS

reaction [58]. A band at 1595 cm^{-1} and a smaller band at 1390 cm^{-1} were assigned to formate species acting as the intermediate for methanation reaction [18]. Furthermore, distinguishable peaks at 3017 and 2906 cm^{-1} were corresponding to the vibration bands of CH_4* and CH_3* species [17]. Upon heating up to 450 ^oC in He flow, the band of CO* adsorbates disappeared quickly while the rest peaks were still recognizable, indicating the preferential desorption of CO* species from the catalyst surface. After switching the feeding gas to 10% H_2/He, the residual surface species disappeared in less than 30 min. The order in peak disappearance substantiated that the surface intermediates in methanation pathway such as CH_4*, CH_3* and formate species possessed a stronger interaction with the active sites of the catalyst, as compared with CO* intermediates in rWGS pathway. This result strongly supported that 1 wt% Ru/Al_2O_3 catalyst preferred the transformation of CO_2 to CO via rWGS process rather than CH_4 formation. It is also in agreement with relatively lower value of E_a in kinetic measurements (73.6 and 67.1 eV for CH_4 and CO formation, respectively).

By combining with the kinetic analysis, the characterizations of surface structures and the monitoring of the active intermediate species during the CO_2 reduction reaction, the catalytic selectivity switching between CH_4 and CO productions over Ru/Al_2O_3 catalysts should be determined by the Ru sites and Ru-Al_2O_3 interfacial sites. To gain an understanding of the reasonable mechanisms in CO_2 reduction reaction, the DFT calculations were performed over two representative

structural models of Ru/Al_2O_3. Based on the characterization results, the fully dehydroxylated (100) terminations of γ-Al_2O_3 were chosen as support surface. To simulate the 3D nanocluster model of Ru, the Ru_{35} nanocluster was built and stabilized on the γ-Al_2O_3(100) surface by bridging through Ru-Al and Ru-O bonds, with a bond length of 2.55-2.60 and 1.98-2.07 Å, respectively (Fig. 9A). A monolayer of Ru_9 with nine Ru atoms dispersed on the same γ-Al_2O_3(100) surface served as the second model (Fig. 9B). The Ru_9/Al_2O_3 structure model after relaxation was a no-plane monolayer in which the bond length of Ru-Al and Ru-O are 2.50-2.53 Å and 1.89-2.04 Å, respectively. The slight difference of bond lengths between two models indicated that γ-Al_2O_3 surface owned a stronger interaction with Ru_9 monolayer sites than with Ru_{35} nanoclusters. The calculated reaction pathways for CO_2 methanation and rWGS were shown in Fig. 10 and Fig. 11, respectively. Noticeably, H_2 dissociation on supported Ru sites was not a rate-limiting step because the fast rates to reach equilibrium during CO_2 hydrogenation reaction [59]. In addition, the adsorption of CO_2 was remarkably stronger over Ru_9/Al_2O_3 than that over Ru_{35}/Al_2O_3 for the initial step in both hydrogenation pathways. The dissociation of CO_2 can also be accelerated over monolayer Ru_9 sites rather than Ru_{35} nanocluster sites. More negative charges can be transferred to CO_2* species adsorbed on monolayer Ru_9 sites with the aid of direct electron contribution from the underneath oxide support [28, 60].

Specifically, the route of CH_4 formation started with the formation of HCOO* species [7,18] and stepwise hydrogenation into HCOOH* and H_2COOH* [61-63]. As a result of the cleavage of the C-OH bond, the dissociation of H_2COOH* led to the formation of H_2CO* and OH*, followed by further hydrogenation of H_2CO* into H_3CO* and OH* into H_2O*. The subsequent reaction step was the cleavage of the C-O bond in H_3CO* to produce H_3C* and O*, then the ultimate formation of CH_4 and H_2O via one more hydrogenation step. The rate-limiting step of the CH_4 route was the dissociation step of H_2COOH* species. The predicted energy barrier in the step was 0.69 eV (66.5 kJ/mol) and 0.80 eV (77.1 kJ/mol) for Ru_{35} and Ru_9 model, respectively. For the CO production via rWGS reaction pathway, CO_2 adsorbed on the top sites of the Ru_{35} nanocluster directly dissociates into CO* and O*, which was the rate-determining step holding a reaction energy of -0.88 eV (-84.9 kJ/mol) and an energy barrier of 0.84 eV (81.0 kJ/mol). In contrast, the energy barrier on monolayer Ru_9/Al_2O_3 model was 0.71 eV (68.5 kJ/mol), which was appreciably lower than that on Ru_{35}/Al_2O_3.

For the competitive pathways of methanation and rWGS in CO_2 hydrogeantion reaction on Ru/Al_2O_3 catalysts with different Ru loadings, the variation trends in both the catalytic selectivity and the E_a value can be strongly supported by the calculated energy profiles. It suggested that the 3D nanocluster Ru_{35}/Al_2O_3 model favored the formation of CH_4 and the monolayer Ru_9/Al_2O_3 model preferred the formation of CO. These two structural models were co-existed in 1% Ru/Al_2O_3 catalyst, while the

increasing Ru loading led to the almost exclusive generation of large 3D particles, which resembled the Ru_{35}/Al_2O_3 model in 3% Ru/Al_2O_3 catalysts. This was helpful to explain why the reaction rate in CH_4 formation increased and that in CO formation reaction was suppressed with the increase of Ru loadings.

3.4 Oxygen-exchange between CO_2 and bridged Ru-O-Al interface

There was an interesting finding towards the catalytic reaction pathway based on the DFT calculations. In the case of CO_2 activation catalyzed over Ru_9/Al_2O_3 model, O* species were dissociated from CO_2 on an interfacial Ru sites (Ru-O-Al) and then easily bridged with the Lewis acid center of Al atoms to form a new Ru-O-Al bond (structure IN1, see Fig. 11), which was an exothermic step with an energy reduction of 0.34 eV (32.8 kJ/mol). The following step was the hydrogenation of an interfacial O atom to form OH* with an energy barrier of 0.31 eV. Then, the further hydrogenation of OH* led to the formation of H_2O with an energy barrier of 0.29 eV. As a consequence, a dynamic incorporation of the interfacial O atom in the bridge Ru-O-Al bond into the final products would easily occur in CO_2 hydrogenation reaction.

The isotope-labeling measurements were carried out on 1% Ru/Al_2O_3 catalyst to clarify the oxygen-exchange process between CO_2 and Ru-O-Al bridge bond. $C^{18}O_2$ gas (^{18}O-95% purity) was used to replace $C^{16}O_2$ under identical reaction conditions and an online mass spectrometer was connected to monitor the mass signals of gaseous products. The isotope-exchange CO_2 reduction reaction started from H_2

introducing (H_2:$C^{18}O_2$= 4:1) when stable signals were reached for the feeding $C^{18}O_2$/He gas. All major gaseous products of both methanation and rWGS in CO_2 hydrogenation were detected on MS spectra, as shown in Fig. 12A. CH_4 and isotopic $C^{18}O$ and $H_2{}^{18}O$, dominated the product distribution, while a small amount of $C^{16}O$ and $H_2{}^{16}O$ have also generated during catalytic reaction, partially due to the co-feeding of $C^{16}O_2$ gas (5%). It should to be emphasized that prominent peaks were emerged on the signal of $H_2{}^{16}O$ (m/z=18) at the initial stage (~5 min) and subsequently equilibrium state was regained. The signal intensity ratio of $H_2{}^{16}O$ (m/z=18) to $H_2{}^{18}O$ (m/z=20) was considerably larger than 5%:95% (the ratio of $C^{16}O_2$:$C^{18}O_2$ in feeding gas) within the first five min, suggesting that ^{18}O-free $H_2{}^{16}O$ was not entirely produced from the hydrogenation reaction of $C^{16}O_2$ impurity with 5% concentration. To further verify the origin of $H_2{}^{16}O$ product, the second reaction run with $C^{18}O_2$ was performed after consecutive treatment of He and H_2/He purgation to remove residual surface species. It was observed that such distinct peak for $H_2{}^{16}O$ (m/z=18) was no longer present in the second run, as shown in Fig. 12B. In addition, similar patterns were obtained on signal channel at m/z 17, which was the main fragment of $H_2{}^{16}O$ that was free from the interferences. These results clearly demonstrated that there were interfacial ^{16}O species on 1% Ru/Al_2O_3 catalyst involving in the exchanging with ^{18}O atoms in $C^{18}O_2$ for producing of $H_2{}^{16}O$ during the initial hydrogenation reaction.

It is reasonably considered that ^{18}O atoms could be left on the interfacial Ru-^{18}O-Al bonds in the spent Ru/Al_2O_3 catalyst after isotopic oxygen-exchange reaction. 18O-free $C^{16}O_2$ hydrogenation reaction was performed over the possibly ^{18}O-labeled 1% Ru/Al_2O_3 catalyst to reveal the role of interfacial bridge oxygen species. When hydrogenation started with sampling of H_2 into $C^{16}O_2$/He gas flow, the signal of $H_2{}^{18}O$ (m/z=20) kept flat for the pristine catalyst, whereas the signal rose a peak immediately for the used catalyst, indicating a substantial yield of $H_2{}^{18}O$ in the $C^{16}O_2$ reduction reaction (Fig. 13A). The expected production of $C^{16}O$ (m/z=28) and CH_4 (m/z=15) was also observed, as shown in Fig. 13B. Furthermore, the MS signals of $C^{18}O$ (m/z=30) and $C^{18}O_2$ (m/z=48) were absent during the reaction, which fully excluded the possibility that the ^{18}O atom of $H_2{}^{18}O$ was originated from gaseous or surface residual $C^{18}O_2$. Based on the above isotope-labeling transient analyses, we expected that $H_2{}^{18}O$ is derived from the incorporation of ^{18}O atoms in interfacial Ru-^{18}O-Al bonds that was produced via the oxygen-exchange process during the first run of $C^{18}O_2$ hydrogenation reaction.

Combined with the isotope-exchange experimental evidences and the theoretic calculation results, CO_2 preferred to be activated and converted into CO on the monolayer Ru sites that directly interacted with the γ-Al_2O_3 support by following the rWGS pathway. Noticeably, the activated dissociation of CO_2 on the monolayer Ru sites left an active O* that further bridges with adjacent Al site of the support to form a ‘new’ interfacial Ru-O-Al bond, achieving the oxygen-exchange between CO_2 and

Ru-Al_2O_3 interface. The illustration of ambient pressure CO_2 hydrogenation reaction catalyzed by Ru/Al_2O_3 catalysts was proposed in Scheme 1.

The rWGS reaction, as the reverse process of water-gas shift, was generally considered as a kind of interfacial structure-sensitive reaction. For instance, the Pt-O_v-Ti^{3+} species formed at the interface between Pt and reducible TiO_2 support was identified as the active sites for the CO formation [64]. According to the analyses of in-situ DRIFTs spectroscopy and microcalorimetry measurements, Pt-O(OH)-K interfaces were evidenced as the primary active sites to achieve CO_2 activation and CO production via bridge-bonded formates intermediates [65]. Similarly, atomically dispersed Rh sites received the directly transferred electrons from the interface with TiO_2 support, favoring the rWGS reaction route in CO_2 hydrogenation, and a strong correlation was obtained between the TOF_{rWGS} value and the fraction of isolated Rh sites [47]. The finding of interfacial oxygen-exchange during the CO_2 activation in this work provides a novel insight into the catalytic effects of the metal-oxide interfaces.

4. Conclusions

In summary, different structure types of Ru sites on γ-Al_2O_3 were prepared via varying the Ru weight loadings and were identified by the comprehensive analyses of H_2-O_2 titration, STEM, EXAFS and CO adsorption IRAS measurements. The monolayer and 3D nanocluster sites of Ru metals are co-existed in 1% Ru/Al_2O_3 catalyst while the latter predominates over 2% and 3% Ru/Al_2O_3 catalysts. By

integrating kinetic measurements and theoretical calculations, the rWGS route to form CO preferentially occurs on monolayer Ru sites, while the methanation route to form CH_4 is in favor of relatively larger 3D Ru nanoclusters. In addition, a dynamic oxygen-exchange process between CO_2 and interfacial Ru-O-Al bond in monolayer Ru-catalyzed rWGS reaction was validated by theoretical calculation results and experimental isotope-labeling studies. The dissociative adsorption of CO_2 at monolayer Ru sites leaves O* species to facilely bridge with the surface Al sites from the γ-Al_2O_3 support, building new interfacial Ru-O-Al bonds via the oxygen-exchange process. The observation in this work highlights the catalytic effects of the active metal-support interfaces in the effective activation of CO_2 for the exploration of the supported metallic catalysts.

Acknowledgments

The authors thank Prof. Hong He and Prof. Yunbo Yu for the help in EXAFS and isotope-exchange analyses. We are grateful for financial support from the Jiangsu Provincial Department of Education and Natural Science Foundation (17KJB150021 and BK20170986). We also thank the support from Campus for Research Excellence and Technological Enterprise (CREATE) program of National Research Foundation (NRF) in Singapore.

References

[1] W. Wang, S. Wang, X. Ma, J. Gong, Recent advances in catalytic hydrogenation of carbon dioxide, Chem. Soc. Rev. 40 (2011) 3703-3727.

[2] M. Aresta, A. Dibenedetto, A. Angelini, Catalysis for the valorization of exhaust carbon: From CO_2 to chemicals, materials, and fuels. Technological use of CO_2, Chem. Rev. 114 (2014) 1709-1742.

[3] M. Behrens, Methanol synthesis over Cu/ZnO/Al_2O_3: The active site in industrial catalysis, Science 336 (2012) 893-897.

[4] P. Gao, S. Li, X. Bu, S. Dang, Z. Liu, H. Wang, L. Zhong, M. Qiu, C. Yang, J. Cai, W. Wei, Y. Sun, Direct conversion of CO_2 into liquid fuels with high selectivity over a bifunctional catalyst, Nat. Chem. 9 (2017) 1019-1024.

[5] J. Graciani, K. Mudiyanselage, F. Xu, A.E. Baber, J. Evans, S.D. Senanayake, D.J. Stacchiola, P. Liu, J. Hrbek, J.F. Sanz, J.A. Rodriguez, Highly active copper-ceria and copper-ceria-titania catalysts for methanol synthesis from CO_2, Science 345 (2014) 546-550.

[6] Y. Yan, Y.H. Dai, H. He, Y.B. Yu, Y.H. Yang, A novel W-doped Ni-Mg mixed oxide catalyst for CO_2 methanation, Appl. Catal. B-Environ. 196 (2016) 108-116.

[7] Y. Yan, Y.H. Dai, Y.H. Yang, A.A. Lapkin, Improved stability of Y_2O_3 supported Ni catalysts for CO_2 methanation by precursor-determined metal-support interaction, Appl. Catal. B-Environ. 237 (2018) 504-512.

[8] P. Sabatier, J.B. Senderens, New synthesis of methane, CR Acad. Sci. Paris 134 (1902) 689-691.

[9] X. Wang, H. Shi, J.H. Kwak, J. Szanyi, Mechanism of CO_2 hydrogenation on Pd/Al_2O_3 catalysts: Kinetics and transient DRIFTS-MS studies, ACS Catal. 5 (2015) 6637-6349.

[10] J.N. Park, E.W. Mcfarland, A highly dispersed $Pd-Mg/SiO_2$ catalyst active for methanation of CO_2, J. Catal. 266 (2009) 92-97.

[11] H.Y. Kim, H.M. Lee, J.N. Park, Bifunctional mechanism of CO_2 methanation on $Pd-MgO/SiO_2$ catalyst: Independent roles of MgO and Pd on CO_2 methanation, J. Phys. Chem. C 114 (2010) 7128-7131.

[12] J.H. Kwak, L. Kovarik, J. Szanyi, Heterogeneous catalysis on atomically dispersed supported metals: CO_2 reduction on multifunctional Pd catalysts, ACS Catal. 3 (2013) 2094-2100.

[13] W. Zhen, B. Li, G. Lu, J. Ma, Enhancing catalytic activity and stability for CO_2 methanation on $Ni-Ru/\gamma-Al_2O_3$ via modulating impregnation sequence and controlling surface active species, RSC Adv. 4 (2014) 16472-16479.

[14] A. Beuls, C. Swalus, M. Jacquemin, G. Heyen, A. Karelovic, P. Ruiz, Methanation of CO_2: Further insight into the mechanism over $Rh/\gamma-Al_2O_3$ catalyst, Appl. Catal. B-Environ. 113-114 (2012) 2-10.

[15] S. Carenco, C. Sassoye, M. Faustini, P. Eloy, D.P. Debecker, H. Bluhm, M. Salmeron, The active state of supported ruthenium oxide nanoparticles during xarbon sioxide methanation, J. Phys. Chem. C 120 (2016) 15354-15361.

[16] S. Akamaru, T. Shimazaki, M. Kubo, T. Abe, Density functional theory analysis of methanation reaction of CO_2 on Ru nanoparticle supported on TiO_2(101), Appl. Catal. A-Gen. 470 (2014) 405-411.

[17] A.M. Abdel-Mageed, S. Eckle, H.G. Anfang, R.J. Behm, Selective CO methanation in CO_2-rich H_2 atmospheres over a Ru/zeolite catalyst: The influence of catalyst calcination, J. Catal. 298 (2013) 148-160.

[18] F. Wang, S. He, H. Chen, B. Wang, L. Zheng, M. Wei, D.G. Evans, X. Duan, Active site dependent reaction mechanism over Ru/CeO_2 catalyst toward CO_2 methanation, J. Am. Chem. Soc. 138 (2016) 6298-6305.

[19] J. Jia, C. Qian, Y. Dong, Y.F. Li, H. Wang, M. Ghoussoub, K.T. Butler, A. Walsh, G.A. Ozin, Heterogeneous catalytic hydrogenation of CO_2 by metal oxides: defect engineering-perfecting imperfection, Chem. Soc. Rev. 46 (2017) 4631-4644.

[20] W. Wang, S. Wang, X. Ma, J. Gong, Recent advances in catalytic hydrogenation of carbon dioxide, Chem. Soc. Rev. 40 (2011) 3703-3727.

[21] Y.H. Dai, Y. Wang, B. Liu, Y.H. Yang, Metallic nanocatalysis: An accelerating seamless integration with nanotechnology, Small, 11 (2015) 268-289.

[22] F. Wang, C. Li, X. Zhang, M. Wei, D.G. Evans, X. Duan, Catalytic behavior of supported Ru nanoparticles on the {100}, {110}, and {111} facet of CeO_2, J. Catal. 329 (2015) 177-186.

[23] K. Larmier, W.C. Liao, S.H. Tada, E. Lam, R. Verel, A. Bansode, A. Urakawa, A. Comas-Vives, C. Coperet, CO_2-to-methanol hydrogenation on zirconia-supported

copper nanoparticles: Reaction intermediates and the role of the metal-support interface, Angew. Chem. Int. Ed. 56 (2017) 2318-2323.

[24] B. Mutz, M. Belimov, W. Wang, P. Sprenger, M.-A. Serrer, D. Wang, P. Pfeifer, W. Kleist, J.-D. Grunwaldt, Potential of an alumina-supported Ni_3Fe catalyst in the methanation of CO_2: Impact of alloy formation on activity and stability, ACS Catal. 7 (2017) 6802-6814.

[25] M. Cargnello, C.B. Murray, Control of metal nanocrystal size reveals metal-support interface role for ceria catalysts, Science 341 (2013) 771-773.

[26] L.C. Liu, A. Corma, Metal catalysts for heterogeneous catalysis: From single atoms to nanoclusters and nanoparticles, Chem. Rev. 118 (2018) 4981-5079.

[27] G.N. Vayssilov, Y. Lykhach, A. Migani, T. Staudt, G.P. Petrova, N. Tsud, T. Skála, A. Bruix, F. Illas, K.C. Prince, V.r. Matolın, K.M. Neyman, J. Libuda, Support nanostructure boosts oxygen transfer to catalytically active platinum nanoparticles, Nat. Mater. 10 (2011) 310-315.

[28] M.C. Silaghi, A. Comasvives, C. Copéret, CO_2 activation on Ni/γ-Al_2O_3 catalysts by first-principles calculations: From ideal surfaces to supported nanoparticles, ACS Catal. 6 (2016) 4501-4505.

[29] S. Tada, R. Kikuchi, Mechanistic study and catalyst development for selective carbon monoxide methanation, Catal. Sci. Technol. 5 (2015) 3061-3070.

[30] M. Ahmadi, H. Mistry, B. Roldan Cuenya, Tailoring the catalytic properties of metal nanoparticles via support interactions, J. Phys. Chem. Letter 7 (2016) 3519-3533.

[31] S.J. Tauster, S.C. Fung, R.L. Garten, Strong metal-support interactions. Group 8 noble metals supported on titanium dioxide, J. Am. Chem. Soc. 100 (1978) 170-175.

[32] S.J. Tauster, S.C. Fung, Strong metal-support interactions: Occurrence among the binary oxides of groups IIA-VB, J. Catal. 55 (1978) 29-35.

[33] R. Prins, Hydrogen spillover. Facts and fiction, Chem. Rev. 112 (2012) 2714-2738.

[34] A. Karelovic, P. Ruiz, Improving the hydrogenation function of Pd/γ-Al_2O_3 catalyst by Rh/γ-Al_2O_3 addition in CO_2 methanation at low temperature, ACS Catal. 3 (2013) 2799-2812.

[35] S.W. Li, Y. Xu, Y.F. Chen, W. Z. Li, L.L. Lin, M.Z. Li, Y.C. Deng, Y.C. Deng, X.P. Wang, B.H. Ge, C. Yang, S.Y. Yao, J.L. Xie, Y.W. Li, X. Liu, D. Ma, Tuning the selectivity of catalytic carbon dioxide hydrogenation over iridium/cerium oxide catalysts with a strong metal-support interaction, Angew. Chem. Int. Ed. 56 (2017) 10761-10765.

[36] S.K. Beaumont, S. Alayoglu, C. Specht, W.D. Michalak, V.V. Pushkarev, J. Guo, N. Kruse, G.A. Somorjai, Combining in situ NEXAFS spectroscopy and CO_2 methanation kinetics to study Pt and Co nanoparticle catalysts reveals key insights into the role of platinum in promoted cobalt catalysis, J. Am. Chem. Soc. 136 (2014) 9898-9901.

[37] S. Kattel, W.T. Yu, X.F. Yang, B.H. Yan, Y.Q. Huang, W.M. Wan, P. Liu, J.G. Chen, CO_2 hydrogenation over oxide-supported PtCo catalysts: The role of the oxide support in determining the product selectivity, Angew. Chem. Int. Ed. 55 (2016) 7968-7973.

[38] W. Diao, J.M.M. Tengco, J.R. Regalbuto, J.R. Monnier, Preparation and characterization of Pt-Ru bimetallic catalysts synthesized by electroless deposition methods, ACS Catal. 5 (2015) 5123-5134.

[39] Kresse, Hafner, W. Hauptstrasse, A. Wien, Ab initio molecular dynamics for open-shell transition metals, Pyhs. Rev. B 48 (1993) 13115-13118.

[40] G. Kresse, J. Furthmüller, Efficient iterative schemes for ab initio total-energy calculations using a plane-wave basis set, Pyhs. Rev. B 54 (1996) 11169-11186.

[41] G. Kresse, D. Joubert, From ultrasoft pseudopotentials to the projector augmented-wave method, Pyhs. Rev. B 59 (1999) 1758-1775.

[42] A. Goguet, F.C. Meunier, D. Tibiletti, J.P. Breen, R. Burch, Spectrokinetic investigation of reverse water-gas-shift reaction intermediates over a Pt/CeO_2 catalyst, J. Phys. Chem. B 108 (2004) 20240-20246.

[43] F. Solymosi, A. Erdöhelyi, Hydrogenation of CO_2 to CH_4 over alumina-supported noble metals, J. Mol. Catal. 8 (1980) 471-474.

[44] F. Solymosi, A. Erdöhelyi, T. Bánsági, Methanation of CO_2 on supported rhodium catalyst, J. Catal. 68 (1981) 371-382.

[45] G.D. Weatherbee, C.H. Bartholomew, Hydrogenation of CO_2 on group VIII metals: IV. Specific activities and selectivities of silica-supported Co, Fe, and Ru, J. Catal. 87 (1984) 352-362.

[46] A. Karelovic, P. Ruiz, CO_2 hydrogenation at low temperature over Rh/γ-Al_2O_3 catalysts: Effect of the metal particle size on catalytic performances and reaction mechanism, Appl. Catal. B-Environ. 113-114 (2012) 237-249.

[47] J.C. Matsubu, V.N. Yang, P. Christopher, Isolated metal active site concentration and stability control catalytic CO_2 reduction selectivity, J. Am. Chem. Soc. 137 (2015) 3076-3084.

[48] M. Chen, D. Kumar, C.W. Yi, D.W. Goodman, The promotional effect of gold in catalysis by palladium-gold, Science 310 (2005) 291-293.

[49] J. Shan, M. Li, L.F. Allard, S. Lee, M. Flytzani-Stephanopoulos, Mild oxidation of methane to methanol or acetic acid on supported isolated rhodium catalysts, Nature 551 (2017) 605-608.

[50] J. Aßmann, E. Löffler, A. Birkner, M. Muhler, Ruthenium as oxidation catalyst: bridging the pressure and material gaps between ideal and real systems in heterogeneous catalysis by applying DRIFT spectroscopy and the TAP reactor, Catal. Today 85 (2003) 235-249.

[51] S. Eckle, Y. Denkwitz, R.J. Behm, Activity, selectivity, and adsorbed reaction intermediates/reaction side products in the selective methanation of CO in reformate gases on supported Ru catalysts, J. Catal. 269 (2010) 255-268.

[52] H. Pfnür, D. Menzel, F.M. Hoffmann, A. Ortega, A.M. Bradshaw, High resolution vibrational spectroscopy of CO on Ru(001): The importance of lateral interactions, Surf. Sci. 93 (1980) 431-452.

[53] M.F. Brown, R.D. Gonzalez, An infrared study of the adsorption of carbon monoxide on the reduced and oxidized forms of silica supported ruthenium, J. Phys. Chem. 80 (1976) 1731-1735.

[54] G.H. Yokomizo, C. Louis, A.T. Bell, An infrared study of CO adsorption on reduced and oxidized Ru/SiO_2, J. Catal. 120 (1989) 1-14.

[55] A.M. Abdelmageed, D. Widmann, S.E. Olesen, I. Chorkendorff, J. Biskupek, R.J. Behm, Selective CO methanation on Ru/TiO_2 catalysts: Role and influence of metal-support interactions, ACS Catal. 5 (2015) 6753-6763.

[56] P. Winslow, A.T. Bell, Application of transient response techniques for quantitative determination of adsorbed carbon monoxide and carbon present on the surface of a ruthenium catalyst during Fischer-Tropsch synthesis, J. Catal. 86 (1984) 158-172.

[57] A.M. Karim, V. Prasad, G. Mpourmpakis, W.W. Lonergan, A.I. Frenkel, J.G. Chen, D.G. Vlachos, Correlating particle size and shape of supported $Ru/\gamma\text{-}Al_2O_3$ catalysts with NH_3 decomposition activity, J. Am. Chem. Soc. 131 (2009) 12230-12239.

[58] A.M. Abdel-Mageed, S. Eckle, D. Widmann, R.J. Behm, Water assisted dispersion of Ru nanoparticles: The impact of water on the activity and selectivity of supported Ru catalysts during the selective methanation of CO in CO_2-rich reformate, J. Catal. 335 (2016) 79-94.

[59] X. Wang, Y. Hong, H. Shi, J. Szanyi, Kinetic modeling and transient DRIFTS-MS studies of CO_2 methanation over Ru/Al_2O_3 catalysts, J. Catal. 343 (2016) 185-195.

[60] D.C. Upham, A.R. Derk, S. Sharma, H. Metiu, E.W. Mcfarland, CO_2 methanation by Ru-doped ceria: The role of the oxidation state of the surface, Catal. Sci. Technol. 5 (2015) 1783-1791.

[61] J. Ye, C. Liu, D. Mei, Q. Ge, Active oxygen vacancy site for methanol synthesis from CO_2 hydrogenation on In_2O_3(110): A DFT study, ACS Catal. 3 (2013) 1296-1306.

[62] Y. Yang, M.G. White, P. Liu, Theoretical study of methanol synthesis from CO_2 hydrogenation on metal-doped Cu(111) surfaces, J. Phys. Chem. C 116 (2012) 248-256.

[63] Y. Yang, J. Evans, J.A. Rodriguez, M.G. White, P. Liu, Fundamental studies of methanol synthesis from CO_2 hydrogenation on Cu(111), Cu clusters, and Cu/ZnO(0001), Phys. Chem. Chem. Phys. 12 (2010) 9909-9917.

[64] P.G. Blakeman, E.M. Burkholder, H.Y. Chen, J.E. Collier, J.M. Fedeyko, H. Jobson, R.R. Rajaram, The role of pore size on the thermal stability of zeolite supported Cu SCR catalysts, Catal. Today 231 (2017) 312-318.

[65] X.L. Yang, X. Su, X.D. Chen, H.M. Duan, B.L. Liang, Q.G. Liu, X.Y. Liu,Y.J. Ren, Y.Q. Huang, T. Zhang, Promotion effects of potassium on the activity and selectivity of Pt/zeolite catalysts for reverse water gas shift reaction, Appl. Catal. B-Environ. 216 (2017) 95-105.

Table 1. Structural properties of Ru/Al_2O_3 catalysts.

Ru/Al_2O_3 Catalyst	Dispersion[a] (%)	CN[b]	d[b](nm)	Dispersion[b] (%)	Fraction of surface Ru sites[c]		
					monolayer	periphery	nanocluster
1%	44.5	6.51±0.4	0.94±0.10	71.6±7.6	45.4%	10.0%	44.6%
2%	35.1	7.29±0.4	1.27±0.10	52.7±4.2	6.8%	9.7%	83.5%
3%	32.2	7.43±0.4	1.32±0.10	50.8±4.2	1.1%	8.4%	90.8%

[a]Dispersion of surface Ru particles obtained from H_2-O_2 titrations.

[b]Results from EXAFS analyses. CN: Ru-Ru first shell coordination number; d and dispersion of Ru particles were calculated based on semispherical structure model;

[c]Calculated based on IRAS of CO adsorption.

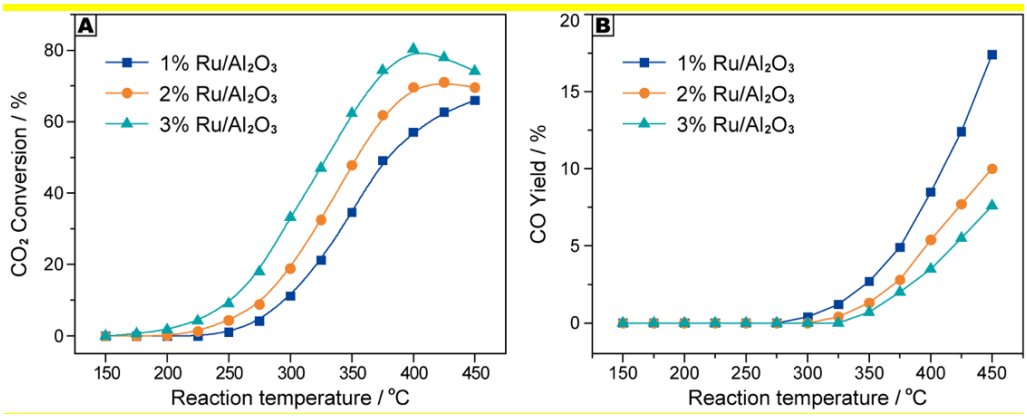

Fig. 1. The catalytic hydrogenation performance (A) CO_2 conversion and (B) CO yield of 1%, 2% and 3% Ru/Al_2O_3 catalysts as a function of reaction temperature.

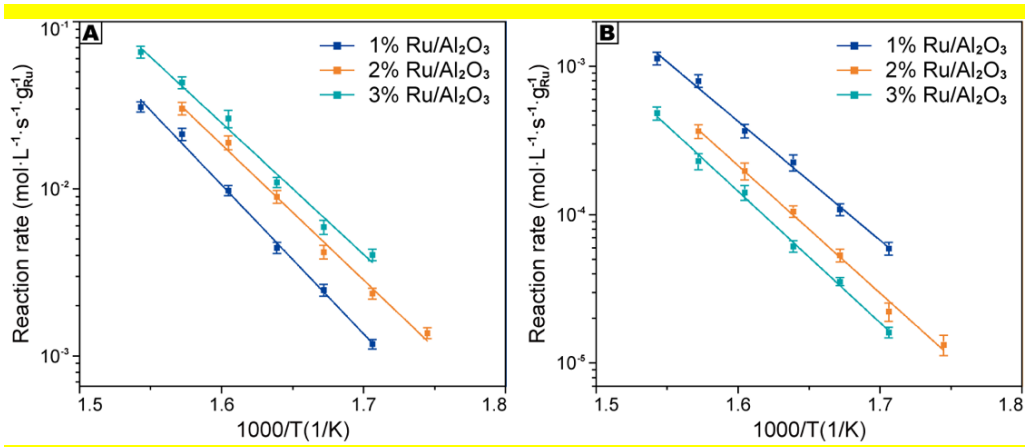

Fig. 2. Arrhenius plots of (A) CH_4 and (B) CO formation rates over Ru/Al_2O_3 catalysts.

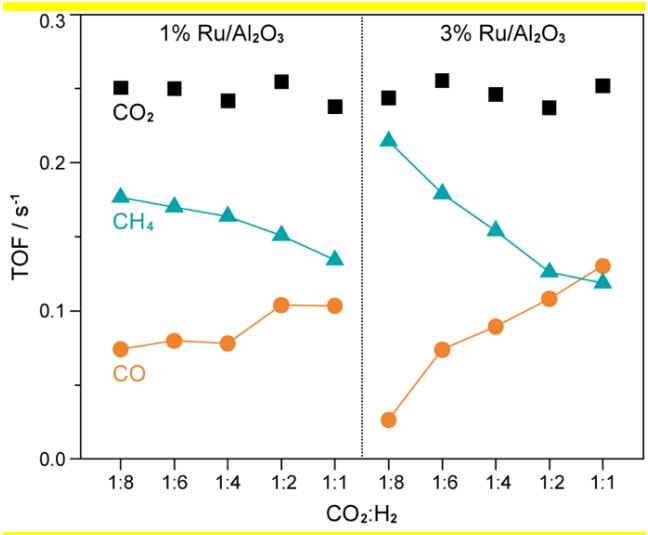

Fig. 3. The TOF for conversion of CO_2, production of CO and CH_4 over 1% and 3% Ru/Al_2O_3 catalysts as a function of CO_2:H_2 ratio.

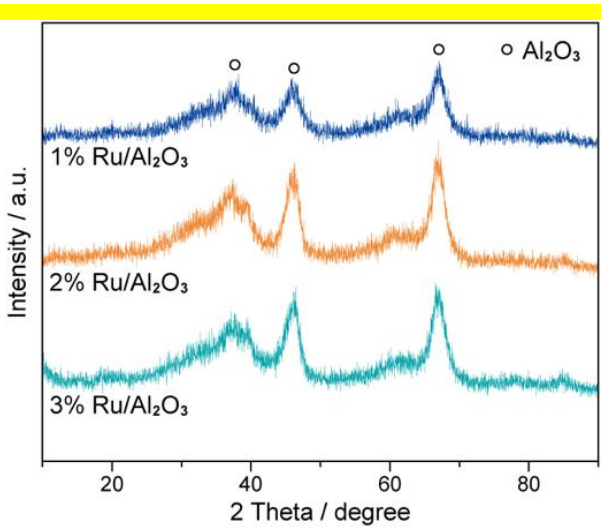

Fig. 4. XRD patterns of Ru/Al_2O_3 catalysts.

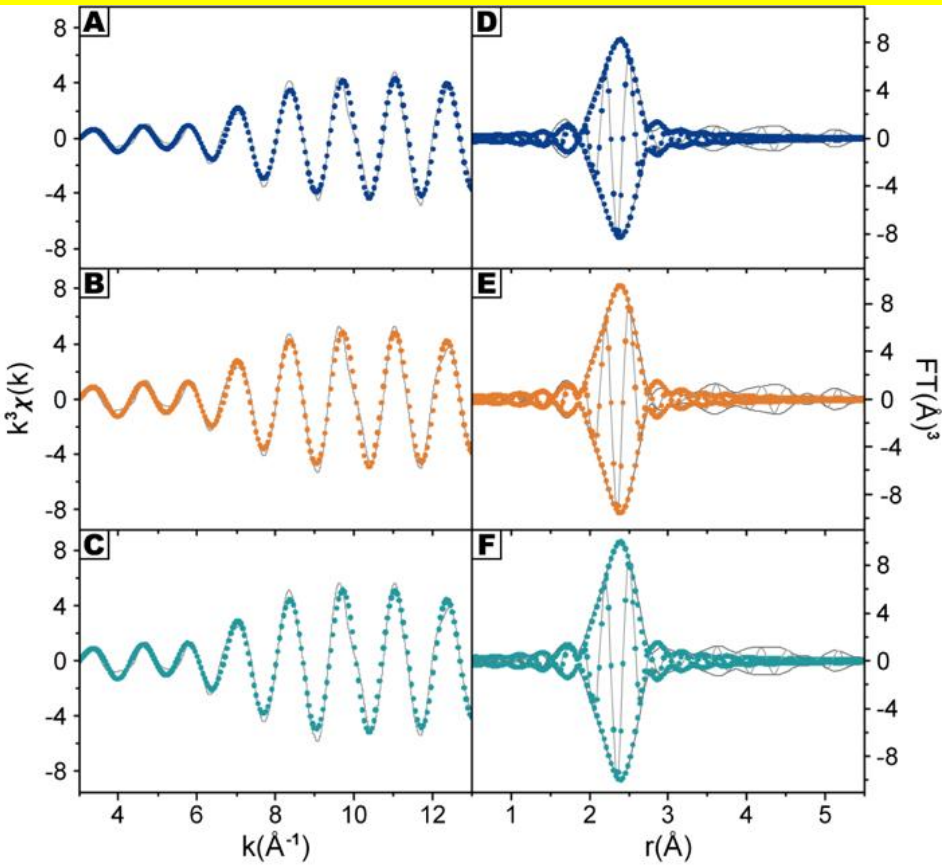

Fig. 5. k^3-weighted χ function and corresponding Fourier transforms obtained on 1% Ru/Al_2O_3 (A and D), 2% Ru/Al_2O_3 (B and E) and 3% Ru/Al_2O_3 (C and F). Solid lines are EXAFS data, and dashed lines are the fits.

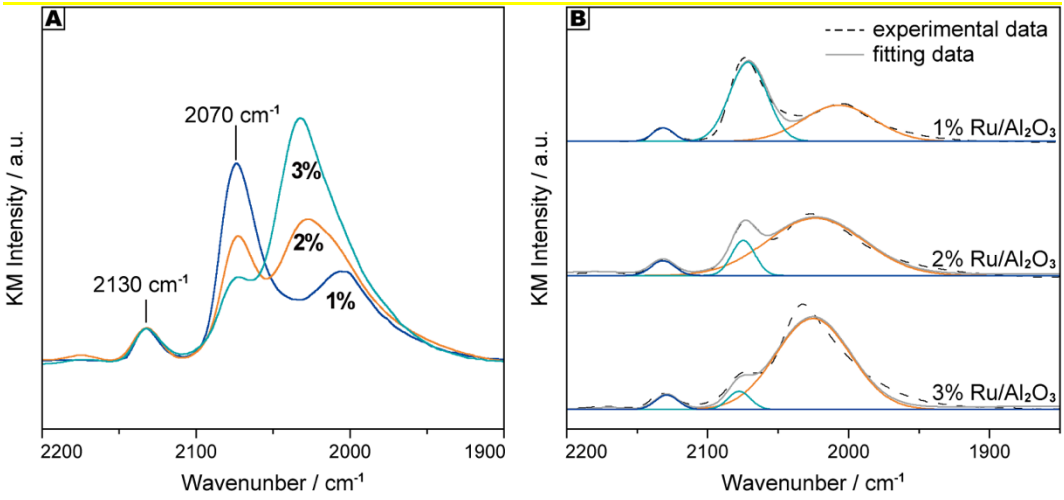

Fig. 6. IRAS spectra for CO adsorption (A) and the deconvoluted data (B) of Ru/Al_2O_3 catalysts.

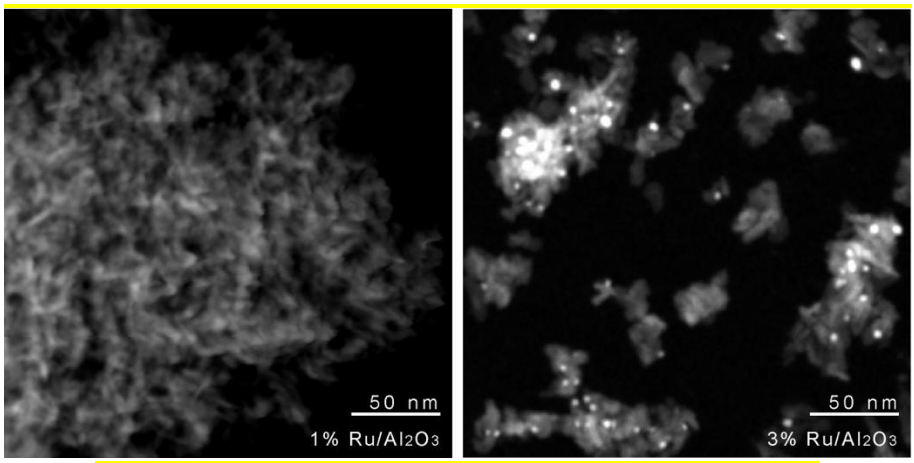

Fig. 7. STEM images of 1% and 3% Ru/Al_2O_3 catalysts.

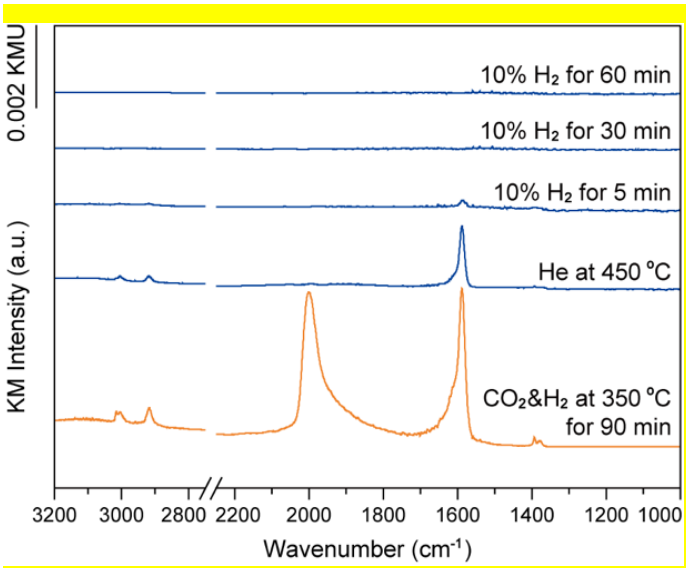

Fig. 8. In-situ DRIFTs spectra collected when the 1% Ru/Al_2O_3 (initially in H_2 and CO_2 flow at 350 ^oC for 90 min) was heated up to 450 ^oC in He at a ramp of 20 ^oC/min, which was then exposed to 10% H_2/He and held there for 5, 30 and 60 min.

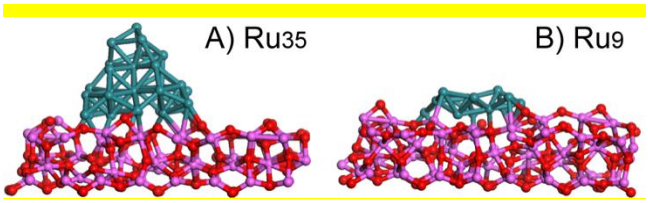

Fig. 9. The optimized model structures of (A) 3D nanocluster Ru_{35}/Al_2O_3 and (B) monolayer Ru_9/Al_2O_3.

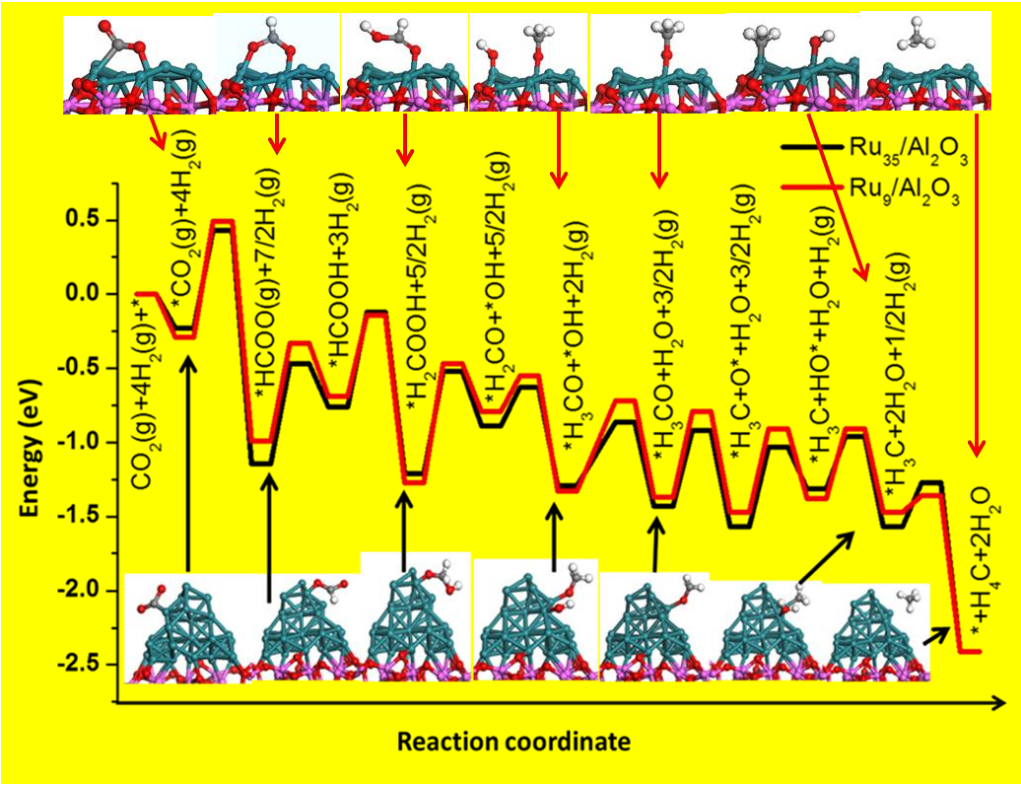

Fig. 10. Potential energy profiles for CO_2 hydrogenation to CH_4 on Ru_{35}/Al_2O_3 and Ru_9/Al_2O_3 models.

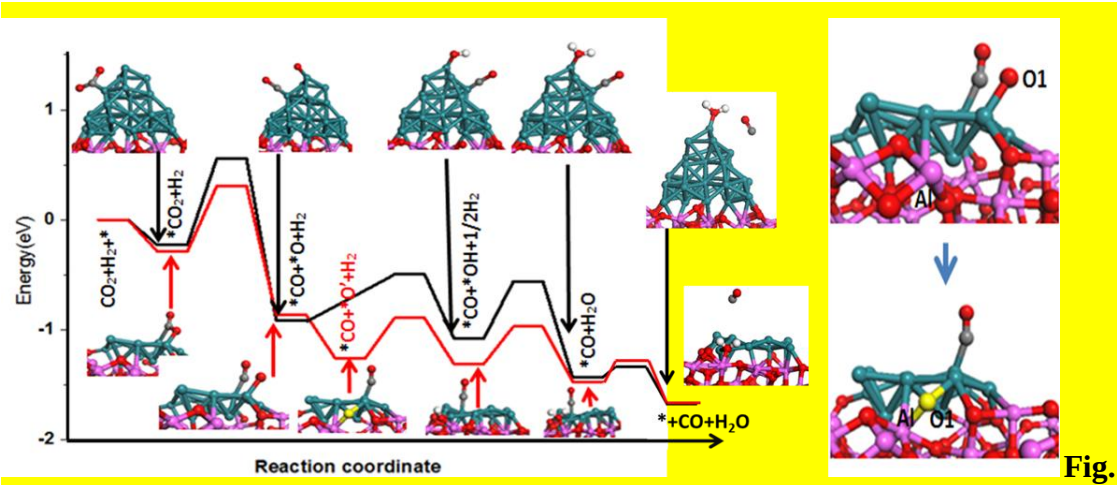

Fig. 11. Potential energy profiles for CO_2 hydrogenation to CO on Ru_{35}/Al_2O_3 and Ru_9/Al_2O_3, along with the structure IN1 (as the right).

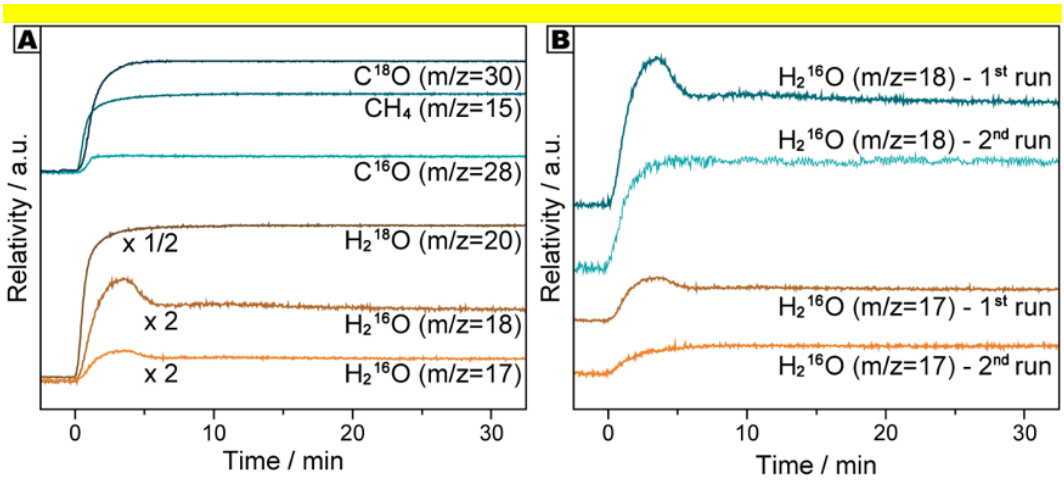

Fig. 12. The MS signals of (A) $H_2{}^{16}O$ (m/z=17, 18) during isotope exposure for two consecutive runs; (B) MS signals in the first run when H_2 was introduced into $C^{18}O_2$/He over pristine 1wt% Ru/Al_2O_3 catalysts.

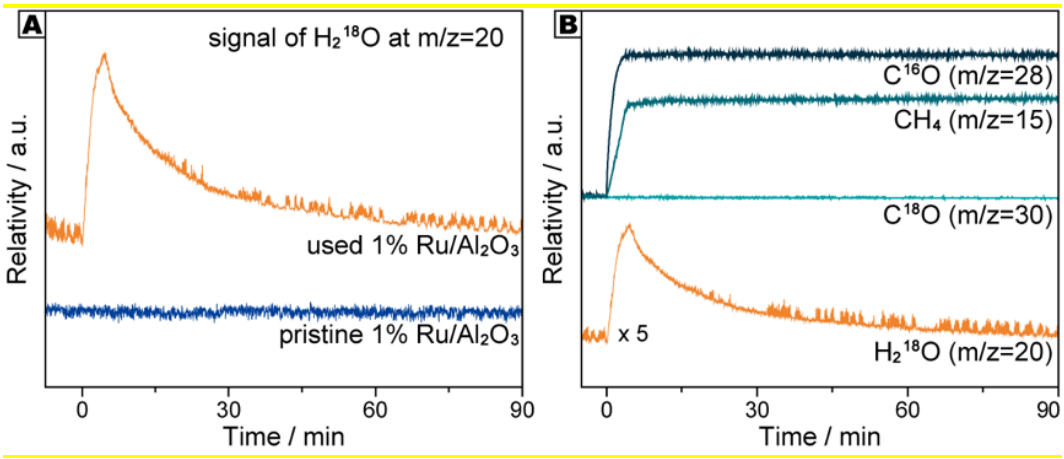

Fig. 13. The MS signals of (A) $H_2{}^{18}O$ (m/z=20) when H_2 was introduced into $C^{16}O_2$/He over used and pristine 1% Ru/Al_2O_3 catalysts; (B) The MS signals as a function of time when H_2 was added into the feed gas of $C^{16}O_2$/He over 1% Ru/Al_2O_3 at 350 ^oC, which is previously exposed to $C^{18}O_2$ and H_2 for 90 min at 350 ^oC.

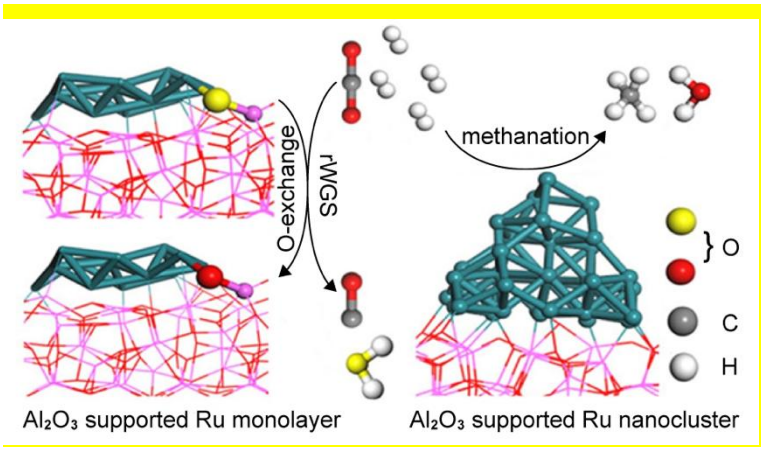

Scheme 1. Schematic illustration of CO_2 hydrogenation to form CO and CH_4 over Ru/Al_2O_3 catalyst.

Ru/Al_2O_3 catalyzed CO_2 hydrogenation: Oxygen-exchange on metal-support interfaces

Yong Yan[a,b], Qiaojuan Wang[a], Chunyang Jiang[a], Di Lu[a], Yihu Dai[a,*], Hongming Wang[c,*], Yanhui Yang[a,*]

[a]Institute of Advanced Synthesis, School of Chemistry and Molecular Engineering, Jiangsu National Synergetic Innovation Center for Advanced Materials, Nanjing Tech University, Nanjing 211816, China

[b]School of Chemical and Biomedical Engineering, Nanyang Technological University, Singapore 637459, Singapore

[c]Institute for Advanced Study and Department of Chemistry, Nanchang University, Xuefu Dadao 999, Nanchang 330031, China

Corresponding authors:

*E-mail: ias_yhdai@njtech.edu.cn (Dr. Y. H. Dai)

*E-mail: hongmingwang@ncu.edu.cn (Prof. H. M. Wang)

*E-mail: yhyang@njtech.edu.cn (Prof. Y. H. Yang)

Abstract

The metal-support interfaces of metallic nanoparticles supported on oxide determine the activated dissociation of CO_2 in CO_2 hydrogenation. It also guides the catalytic pathway towards either CO_2 methanation or reverse water-gas shift (rWGS). In this work, Ru/Al_2O_3 catalysts with different Ru structural configurations were prepared by controlling the Ru weight loadings, which revealed the structure-dependence of production rates for CO and CH_4 formation with different apparent activation energies. Based on the characterization results, two catalyst models were setup: the Ru_9/Al_2O_3 model consisted an interface of monolayer Ru sites tightly contacted with γ-Al_2O_3 supports, and the Ru_{35}/Al_2O_3 model represented a relatively larger Ru nanocluster supported on γ-Al_2O_3. Theoretical calculations of these two models demonstrated that monolayer Ru sites favored the rWGS route with a relatively low energy barrier for both CO_2 activation and CO formation steps, while Ru nanoclusters preferred methanation route energetically. Furthermore, the combination of theoretical calculations and experimental isotope-exchange measurements suggested that the interfacial O species in Ru-O-Al interfaces acted a critical role in CO_2 activation via oxygen-exchanging with the O atom in the feeding CO_2 and consequently incorporating into the final hydrogenation product.

Keywords: CO_2, methanation, reverse water-gas shift, oxygen exchange, interface

1. Introduction

The catalytic conversion of CO_2 to useful products such as CO or carbon-neutral fuels is an essential reaction process since it involves carbon recycle with fundamental research interest and potential industrial applications as well as the environmental implications [1,2]. In consideration of the thermodynamic stability of CO_2 and the high energy barrier for splitting C=O bond, the effective CO_2 activation deems as a critical step in improving the kinetics for overall reaction. Undoubtedly, it needs the rational design of the promising heterogeneous catalysts based on the mechanistic understandings of CO_2 activation and reaction pathway [3-5].

The hydrogenation of CO_2 at atmospheric pressure is of great significance for CO_2 utilization, which proceeds via either reverse water-gas shift (rWGS) to yield CO or methanation reaction to produce CH_4 [6,7]. Although the processes have been thoroughly studied from the beginning of the 20^{th} century [8], no consensus has been reached for the activation mechanism. A bi-functional mechanism was verified on supported Pd catalysts in which H_2 dissociation on metallic Pd particles and CO_2 activated adsorption on metal oxide support occurred synergistically to produce CH_4 via the formation of carbonates intermediates [9]. As a comparison, the Pd/SiO_2 catalyst without effectively active oxides almost exclusively yielded CO in the CO_2 hydrogenation reaction [10,11]. This concept was further validated by the inactive performance of Pd supported on inert multi-walled carbon nanotubes [12]. In addition, another mechanism of the direct activated dissociation of CO_2 over the metal particles

has been proposed for Ru and Rh catalysts [13-17], which was experimentally observed by both in-situ diffuse reflectance infrared Fourier transform spectroscopy (DRIFTs) and ambient-pressure X-ray photoelectron spectroscopy (XPS) [14,15], and theoretically validated by density function theory (DFT) calculations [16]. Interestingly, both the oxygen vacancy on the support and the metallic Ru particles can serve as the activation sites for CO_2 to form CH_4 over Ru/CeO_2 but via two different reaction pathways [18].

The interface of supported catalyst possesses dual sites of the metal-oxide heterojunction, playing pivotal roles in governing the electronic and chemical structures of the catalysts and the surface reaction process [19-21]. A number of structural factors in the supported metal sites, including the particle size, bimetallic alloying, crystal planes, redox ability and acidity, can finely tune the interfacial effects in the catalytic reactions [22-26]. For instance, smaller nanoclusters gain the characters varying with multiple neighboring sites with versatile geometric and electronic structures, as compared to larger nanoparticles [27]. The acceleration of CO_2 dissociation process at the metal-support interface was observed on the supported catalysts with the optimized metal particle size [28,29]. On the other hand, the support-induced interfacial effects can also allow the tailoring of the electronic structure, the chemical state and the stability of the metal species for the enhancement in the catalytic performance [30]. In hydrogenation chemistry, both the strong metal-support interaction (SMSI) and hydrogen spillover would be subjected to the

interfacial effects [31-34]. The CeO_2 supported metallic Ir nanoparticles select for CH_4 production, while the partially oxidized IrO_x sites that are modulated by a SMSI effect prefer selective production of CO in the hydrogenation of CO_2 [35]. Beaumont et al. have reported that a long-distance hydrogen spillover from Pt to Co sites led the reduction of Co NPs, generating more active sites and therefore dramatically increasing in CH_4 production [36]. By combining experimental characterizations and theoretical calculations, the proper metal-oxide interfaces have been demonstrated to selectively strengthen the binding of C, O-bound and O-bound species, leading to the diverse product selectivity in the CO_2 hydrogenation reaction [37].

Herein, the structure-selectivity relationship and the interfacial oxygen-exchange pathway were presented in γ-Al_2O_3 supported Ru catalyzed CO_2 hydrogenation at atmospheric pressure. Three structural configurations of Ru sites consisting monolayer, periphery and nanocluster were prepared by the control of metallic loadings and carefully characterized. By combining experimental and theoretical analyses, the monolayer Ru sites energetically prefer the rWGS route while the relatively larger Ru nanoclusters prefer the methanation route. Furthermore, the oxygen-exchange between O atom in gaseous CO_2 and the bridged Ru-O-Al interfaces as well as its catalytic effects in the CO_2 activated dissociation have also been demonstrated by isotope-labeling evidences and calculation results.

2. Experimental

2.1 Catalyst preparation

Ru/Al_2O_3 catalysts with metal loadings of 1, 2 and 3 wt% were prepared on commercial γ-Al_2O_3 supports by the incipient wetness impregnation method. Typically, a certain amount of ruthenium (III) acetylacetonate (Sigma-Aldrich) was dissolved in ethanol with the volume decided by the pore volume of the support acquired by nitrogen adsorption-desorption isotherms at -198 °C on a Quantachrome AUTO-SORB-6B static volumetric instrument (~0.8 cm^3/g). The obtained solution was then added dropwise onto the support under intensive mixing. The resulted powder was dried for 12 h at 80 °C and the catalysts were then obtained via calcination at 500 ^oC for 2 h under 10% H_2/He with a flow rate of 100 mL/min.

2.2 Catalyst characterizations

H_2-O_2 titration was carried out on a Micromeritics Autochem II 2920 instrument equipped with a TCD detector to measure the amount of surface metal sites. Typically, 100 mg of catalysts were loaded into a U-tube reactor for analysis. All samples were pretreated in H_2 flow for 60 min at 500 ^oC and then purged with Ar for 30 min before cooling to 30 ^oC in the same atmosphere. A gas flow of 10% O_2/Ar was passed over the samples for 30 min to allow the complete coverage of formed O species on the metal surfaces. After switching the feeding gas to pure Ar, sample was heated up to 250 ^oC and held there until the signal was stable. Subsequently, consecutive pulses of 10% H_2/Ar were dosed at 5 min intervals to consume all the surface oxygen. The exposed Ru surface sites was calculated with the assumed stoichiometry of H_2/Ru = 5/2 [38].

Scanning transmission electron microscopy (STEM) analysis was carried out on a FEI Tecnai G2 F20 S-TWIN system operated at 200 kV. The adsorption of CO accompanied by infrared reflection absorption spectroscopy (IRAS) at 25 ^{o}C was performed on a FTIR spectrometer (Nicolet iS50) equipped with a smart collector and a MCT/A detector cooled by liquid nitrogen. Prior to each experiment, the sample was pretreated at 500 ^{o}C for 60 min in 10% H_2/He and then cooled down in He flow to 25 ^{o}C. The background spectrum was collected after 60 min in He purge, followed by introducing 10% CO/He flow to start the chemisorption. After 30 min in CO/He, the sample was purged in He for another 30 min and the resulted spectrum was then acquired. All spectra were recorded by accumulating 100 scans with a resolution of 4 cm^{-1}.

2.3 Kinetic measurements

For kinetic measurements, a desired amount of catalysts was loaded into a fix-bed quartz tube micro-reactor, which was in-situ reduced in a 10% H_2/He gas flow of 100 mL/min at 500 ^{o}C for 60 min, and then kept at a reaction temperature to measure the activity. The measurements were carried out at atmospheric pressure by passing a gaseous mixture of CO_2 (5%) and H_2 (20%) in He balance at a total flow rate of 100 mL/min. The inlet and outlet flows were analyzed by an on-line gas chromatograph (Agilent 6890) equipped with both a FID and a TCD detector. The sampling data were collected when reaction reached a steady state (~60 min after

reaching the desired reaction temperature). The kinetic measurement was performed by keeping the CO_2 conversion below 15%.

2.4 First-principles calculations

Density functional theory (DFT) calculations were carried out to investigate the catalytic reaction mechanism of CO_2 hydrogenation on Al_2O_3-supported Ru clusters. The Al_2O_3-supported Ru_{35} cluster and single layer Ru_9 cluster were constructed by binding the Ru_{35} and single layer Ru_9 cluster onto a γ-Al_2O_3(100) surface. The unit cell of the amorphous Al_2O_3 surface for periodic DFT calculation has a dimension of 10 × 13 × 18 Å, with a vacuum space of 15 Å. All the calculations were carried out using the GGA functional with a projector-augmented wave basis set implemented in the Vienna Ab initio Simulation Package [39-41]. The energy cutoff of 350 eV was used. For the Al_2O_3 supported catalyst, atoms in the top two layers of the Al_2O_3 slab and adsorbed species were allowed to relax while the bottom layers of the Al_2O_3 slab were kept static.

2.5 Isotope-exchange experiments

For the isotope-exchange experiments, the as-calcined catalyst was loaded into a fixed bed quartz reactor, followed by reducing at 500 ° C for 60 min under 10% H_2 /He (flow rate=50 mL/min). Pure He or different mixtures, 1% $C^{18}O_2$ (95%-^{18}O, Linde North America Inc.) or $C^{16}O_2$, and/or 4% H_2 diluted in He, were switched and introduced into the reactor. The gases at the outlet of the reactor were analyzed by a mass spectrometer (GAM 300, InProcess Instruments) by following the evolution of

the m/z=48 ($C^{18}O_2$), 15 (CH_4), 20 ($H_2{}^{18}O$), 18 & 17 ($H_2{}^{16}O$), 30 ($C^{18}O$), 28 ($C^{16}O$) with the response time of the mass spectrometer following a change in gas concentration being less than 2 s.

3. Results

3.1 Catalytic performances and kinetics

There was a hypothesis that the conversion of CO_2-to-CO could be completed via the consequent reaction processes, the formation of surface carbonates from CO_2 adsorption and the release of gaseous CO from the direct interaction between formed carbonates and the surface oxygen species in the metal oxide support [42]. Therefore, the catalytic effects of bare γ-Al_2O_3 support in the CO_2 reduction reaction became one of the first concerns. The reference test was carried out under identical reaction conditions and neither CO nor CH_4 was detected as the product over γ-Al_2O_3 support. The involvement of Ru sites with/without interaction with Al_2O_3 support was essential in the reaction.

Fig. 1 showed dependences of the catalytic performance on reaction temperature in the CO_2 hydrogenation over Ru/Al_2O_3 catalysts with three Ru loadings. Two reaction pathways, CO_2 methanation to form CH_4 and reverse water-gas shift (rWGS) reaction to form CO, competitively occurred in the reaction on these catalysts. The CO_2 conversion curves were presented in Fig. 1A. 3% Ru/Al_2O_3 catalyst showed the superior CO_2 conversion with the onset temperature at approximately 200 ^oC and the maximum conversion of 80% at 400 ^oC. Further increasing reaction temperature led

to the decline in CO_2 conversion due to the thermodynamic equilibrium limitation. Similar curves of CO_2 conversion were obtained on 2% and 1% Ru/Al_2O_3 catalysts, however, higher onset temperatures and lower maximum activities displayed.

With increasing the reaction temperature, the identical variation trend of CH_4 yield with the weight loading of Ru was observed, compared with that of the CO_2 conversion. However, it was a contrary dependency of CO yield (selectivity) with the weight loading of Ru. As shown in Fig. 1B, the formation of CO started at approximately 300 ^oC and increased with ramping temperatures, and the CO yield was the highest over 1% Ru/Al_2O_3 of being 17.4% at 450 ^oC, which was twice of that over 3% Ru/Al_2O_3 catalyst, indicating that CH_4 formation was favored and CO formation was suppressed with increasing Ru loadings.

To measure the specific reaction rates and the apparent activation energies (E_a) of three Ru/Al_2O_3 catalysts in a certain temperature window, less than 15% CO_2 conversions were achieved by regulating the usage amount of the catalysts. The Arrhenius plots for CH_4 and CO formation were separately displayed in Fig. 2A and Fig. 2B. For 3% and 2% Ru/Al_2O_3 catalysts, the E_a value for CH_4 formation was 65.0±3.5 kJ/mol (0.67±0.04 eV) while that for CO formation was 75.0±4.3 kJ/mol (0.78±0.04 eV). The distinctly different E_a values have been observed on 1% Ru/Al_2O_3 catalyst, which the calculated E_a for CH_4 formation increased to 73.6±3.2 kJ/mol (0.76±0.03 eV), and the E_a for CO formation decreased to 67.1±2.7 kJ/mol (0.69±0.03 eV). Comparable results have been reported that E_a of 67.4 and 72.0

kJ/mol were obtained on Ru/Al_2O_3 and Ru/SiO_2 catalysts, respectively [43-45]. There was also an experimental observation that the E_a for CH_4 and CO formation varied with different metal loadings for Pd/Al_2O_3 and Rh/Al_2O_3 catalysts, due to the particle size effects and the different roles of individual active sites [46]. In this study, the different E_a values strongly supported the opposite preference of the production of CO or CH_4 on Ru/Al_2O_3 catalysts with different Ru loadings. It could be expected that different reaction routes proceeded on different active sites during the CO_2 reduction reaction.

The Ru site-specific TOF for CH_4 and CO production was also independently examined over three Ru/Al_2O_3 catalysts under varying CO_2:H_2 ratios and similar level of TOF_{CO2} (approximately 0.25 s^{-1} for total CO_2 conversion) (Fig. 3). When the ratio of CO_2:H_2 was less than the stoichiometric ratio for methanation reaction (1:4), the TOF toward CO formation over 1% $Ru/A_{l2}O_3$ remained constant (~0.08 s^{-1}). As the CO_2:H_2 ratio was increased to more CO_2-rich condition, the TOF of CO formation slightly increased due to the fact that the thermodynamic equilibrium preferred the production of CO rather than CH_4 under the relatively higher CO_2:H_2 ratios. However, for 3% Ru/Al_2O_3 catalyst, the TOF of CO formation increased in direct proportion to the CO_2:H_2 ratio in the full range. The different relationship between the CO production TOF and the CO_2:H_2 ratio was revealed on 1% and 3% Ru/Al_2O_3 catalysts. This result suggested that different types of active Ru sites existed in the two catalysts and the rWGS reaction over Ru catalysts was structure-sensitive process. The

structure-activity relationships in CO_2 reduction reaction catalyzed by Ru/Al_2O_3 with different Ru loadings were further discussed as below.

3.2 Characterizations of Ru surface structures

The dispersions of Ru atoms on catalyst surface were determined from volumetric H_2-O_2 titration measurements via reduction of O_2-precovered Ru surface by 10% H_2/Ar gas at 250 ^oC [38]. The total uptake of H_2 reflected the concentrations of surface Ru sites, which were 2.63×10^{19}, 4.14×10^{19} and 5.71×10^{19} g^{-1} for 1%, 2% and 3% Ru/Al_2O_3 catalysts, respectively. Accordingly, the calculated dispersion of Ru metals decreased with the increase of the Ru weight loading from 1% to 3% (44.5% to 32.2%), as shown in Table 1. As shown in Fig. 4, XRD patterns of three Ru/Al_2O_3 catalysts showed only the diffraction peaks of the γ-phase of commercial Al_2O_3 support. The diffraction peaks corresponding to the metallic Ru^0 and RuO_x species were not discerned, possibly due to the high dispersion of small Ru nanoclusters on γ-Al_2O_3 at low weight loadings.

Fig. 5 showed the k^3-weighted $\chi(k)$ functions (where k was wave number) and corresponding Fourier transforms of EXAFS spectra, providing highly responsive structure information of the local coordination environment of Ru atoms. The bi-shell fitting of Ru-Ru and Ru-O paths can be first ruled out, whereas the single Ru-Ru scattering shell can fit with the measured spectra reasonably, with the resulted structural parameters being presented in Table 1. An increase of CN from 6.51 to 7.29 was observed when Ru loading was changed from 1% to 2%, while the further

increase of Ru loading to 3% only resulted in a marginal increase of the CN to 7.43. The appreciable variation in CN values suggested that there was a prominent structural change for the supported Ru particles from 1% to 2% (3%) Ru/Al_2O_3 catalysts. A correlation between the Ru-Ru first shell CN and the average diameter of Ru particles with *hcp* hemispheric model was reported [44,45]. The increasing CN from 6.51 to 7.43 was corresponding to an increase of the Ru particle size, which equaled to 0.94, 1.27 and 1.32 nm for 1%, 2% and 3% Ru/Al_2O_3 catalysts, respectively. Correspondingly, the dispersions of surface Ru atoms were estimated based on the diameters and the hemispheric structure model, which were 71.6%, 52.7% and 50.8% for 1%, 2% and 3% Ru/Al_2O_3 catalysts, respectively. In contrasted to the results of H_2-O_2 titration that the Ru dispersions of three catalysts are 44.5%, 35.1% and 32.2%, respectively, the values in the range from 50.8% to 71.6% were apparently overestimated, suggesting that the Ru particles in three Ru/Al_2O_3 catalysts did not fully accord with the regular hemispheric structure model. The different structure types may be included for the Ru sites on the γ-Al_2O_3 surface.

The infrared reflection absorption spectroscopy (IRAS) of the chemisorption of CO as the probe molecule on three Ru/Al_2O_3 catalysts was used for providing sensitive structural information of surface Ru sites [47-49]. The IRAS tests were performed at 25 ^{o}C and the spectra were presented in Fig. 6A. Two distinct peaks at high frequencies (HF) of 2130 and 2072 cm^{-1}, along with one at low frequencies (LF) between 2000 and 2050 cm^{-1} were observed over all catalysts. For a better

comparison, the spectra were displayed in Kubelka-Munk (KM) unit and normalized with the peak area at 2130 cm^{-1}.

The LF peak was assigned to the linear CO* ("*" represents the adsorbed species) on top sites of relatively larger three-dimension (3D) Ru nanoclusters that interacted with all surrounding sites by Ru-Ru bonds [50,51]. The blue shift of this peak was caused by the dipole-dipole coupling effect of the adsorbed CO* species with increasing concentrations [52,53]. The two HF peaks at 2130 and 2072 cm^{-1} were associated with CO adsorbed on Ru sites that were perturbed by bonds from the support [53,54]. The peak at 2130 cm^{-1} was ascribed to the symmetric stretches of bi-carbonyl species that adsorbed on the uncoordinated Ru sites at the periphery interface, while the peak at 2072 cm^{-1} was contributed from both the asymmetric stretches of bi-carbonyl species and the vibration of linear adsorbed CO on Ru sites of monolayers [51,53-56]. Therefore, 3D nanoclusters, periphery interface sites and monolayer sites of Ru species were co-existed in Ru/Al_2O_3 catalyst structures. It has also confirmed that ideal hemispheric structure model cannot match with Ru sites in this catalyst system.

A clearly opposite variation tendency of peak intensity for 2070 cm^{-1} peak and LF peak was observed with increasing Ru loadings. To further quantify the surface structural compositions, the IRAS spectra were deconvoluted into Gaussian sub-bands using the coefficient values acquired by Yokomizo et al. [54], as shown in Fig. 6B. Based on the above assignments and analysis method, the distributions of linear

adsorbed CO and bicarbonyls were obtained and the fractions of corresponding Ru sites were listed in Table 1. For three Ru catalysts, the periphery sites of Ru maintained similar proportions. However, the fraction of Ru sites in monolayers has drastically decreased from 45.4% to 6.8% when Ru loading raised from 1% to 2%, while that fraction in 3% Ru/Al_2O_3 was only 1.1%. Conversely, the fraction of top sites in 3D Ru nanoclusters has almost doubled when Ru loading increased from 1% to 2%, while further increasing Ru loading to 3% only resulted in a relatively small increase in the fraction. For 1% Ru/Al_2O_3, both monolayers and 3D nanoclusters with multiple layers were present in an appreciable percentage. For 2% and 3% Ru/Al_2O_3, 3D multilayers dominated the Ru sites. It has been reported that the calcination treatment most likely led to planar Ru sites lying on the γ-Al_2O_3 surface [57]. The HAADF-STEM analyses (Fig. 7) revealed such tendency on 1% Ru/Al_2O_3 catalyst. No formation of Ru nanoparticles was observed in the most investigation area. However, for 3% Ru/Al_2O_3 catalyst, it was so intuitive that small Ru nanoparticles dispersed on the Al_2O_3 support individually.

3.3 Structure-activity relationship

The evolution of the surface intermediate species was monitored by in-situ DRIFT spectra during the CO_2 hydrogenation reaction over 1 wt% Ru/Al_2O_3 catalyst (Fig. 8). The reaction was carried out at 350 ^oC and the equilibrium time was lasted for 90 min under reaction flow of CO_2 and H_2. A clear band at 2000 cm^{-1} was observed, which was ascribed to CO* species serving as the intermediate for rWGS

reaction [58]. A band at 1595 cm^{-1} and a smaller band at 1390 cm^{-1} were assigned to formate species acting as the intermediate for methanation reaction [18]. Furthermore, distinguishable peaks at 3017 and 2906 cm^{-1} were corresponding to the vibration bands of CH_4* and CH_3* species [17]. Upon heating up to 450 ^oC in He flow, the band of CO* adsorbates disappeared quickly while the rest peaks were still recognizable, indicating the preferential desorption of CO* species from the catalyst surface. After switching the feeding gas to 10% H_2/He, the residual surface species disappeared in less than 30 min. The order in peak disappearance substantiated that the surface intermediates in methanation pathway such as CH_4*, CH_3* and formate species possessed a stronger interaction with the active sites of the catalyst, as compared with CO* intermediates in rWGS pathway. This result strongly supported that 1 wt% Ru/Al_2O_3 catalyst preferred the transformation of CO_2 to CO via rWGS process rather than CH_4 formation. It is also in agreement with relatively lower value of E_a in kinetic measurements (73.6 and 67.1 eV for CH_4 and CO formation, respectively).

By combining with the kinetic analysis, the characterizations of surface structures and the monitoring of the active intermediate species during the CO_2 reduction reaction, the catalytic selectivity switching between CH_4 and CO productions over Ru/Al_2O_3 catalysts should be determined by the Ru sites and Ru-Al_2O_3 interfacial sites. To gain an understanding of the reasonable mechanisms in CO_2 reduction reaction, the DFT calculations were performed over two representative

structural models of Ru/Al_2O_3. Based on the characterization results, the fully dehydroxylated (100) terminations of γ-Al_2O_3 were chosen as support surface. To simulate the 3D nanocluster model of Ru, the Ru_{35} nanocluster was built and stabilized on the γ-Al_2O_3(100) surface by bridging through Ru-Al and Ru-O bonds, with a bond length of 2.55-2.60 and 1.98-2.07 Å, respectively (Fig. 9A). A monolayer of Ru_9 with nine Ru atoms dispersed on the same γ-Al_2O_3(100) surface served as the second model (Fig. 9B). The Ru_9/Al_2O_3 structure model after relaxation was a no-plane monolayer in which the bond length of Ru-Al and Ru-O are 2.50-2.53 Å and 1.89-2.04 Å, respectively. The slight difference of bond lengths between two models indicated that γ-Al_2O_3 surface owned a stronger interaction with Ru_9 monolayer sites than with Ru_{35} nanoclusters. The calculated reaction pathways for CO_2 methanation and rWGS were shown in Fig. 10 and Fig. 11, respectively. Noticeably, H_2 dissociation on supported Ru sites was not a rate-limiting step because the fast rates to reach equilibrium during CO_2 hydrogenation reaction [59]. In addition, the adsorption of CO_2 was remarkably stronger over Ru_9/Al_2O_3 than that over Ru_{35}/Al_2O_3 for the initial step in both hydrogenation pathways. The dissociation of CO_2 can also be accelerated over monolayer Ru_9 sites rather than Ru_{35} nanocluster sites. More negative charges can be transferred to CO_2* species adsorbed on monolayer Ru_9 sites with the aid of direct electron contribution from the underneath oxide support [28, 60].

Specifically, the route of CH_4 formation started with the formation of HCOO* species [7,18] and stepwise hydrogenation into HCOOH* and H_2COOH* [61-63]. As a result of the cleavage of the C-OH bond, the dissociation of H_2COOH* led to the formation of H_2CO* and OH*, followed by further hydrogenation of H_2CO* into H_3CO* and OH* into H_2O*. The subsequent reaction step was the cleavage of the C-O bond in H_3CO* to produce H_3C* and O*, then the ultimate formation of CH_4 and H_2O via one more hydrogenation step. The rate-limiting step of the CH_4 route was the dissociation step of H_2COOH* species. The predicted energy barrier in the step was 0.69 eV (66.5 kJ/mol) and 0.80 eV (77.1 kJ/mol) for Ru_{35} and Ru_9 model, respectively. For the CO production via rWGS reaction pathway, CO_2 adsorbed on the top sites of the Ru_{35} nanocluster directly dissociates into CO* and O*, which was the rate-determining step holding a reaction energy of -0.88 eV (-84.9 kJ/mol) and an energy barrier of 0.84 eV (81.0 kJ/mol). In contrast, the energy barrier on monolayer Ru_9/Al_2O_3 model was 0.71 eV (68.5 kJ/mol), which was appreciably lower than that on Ru_{35}/Al_2O_3.

For the competitive pathways of methanation and rWGS in CO_2 hydrogeantion reaction on Ru/Al_2O_3 catalysts with different Ru loadings, the variation trends in both the catalytic selectivity and the E_a value can be strongly supported by the calculated energy profiles. It suggested that the 3D nanocluster Ru_{35}/Al_2O_3 model favored the formation of CH_4 and the monolayer Ru_9/Al_2O_3 model preferred the formation of CO. These two structural models were co-existed in 1% Ru/Al_2O_3 catalyst, while the

increasing Ru loading led to the almost exclusive generation of large 3D particles, which resembled the Ru_{35}/Al_2O_3 model in 3% Ru/Al_2O_3 catalysts. This was helpful to explain why the reaction rate in CH_4 formation increased and that in CO formation reaction was suppressed with the increase of Ru loadings.

3.4 Oxygen-exchange between CO_2 and bridged Ru-O-Al interface

There was an interesting finding towards the catalytic reaction pathway based on the DFT calculations. In the case of CO_2 activation catalyzed over Ru_9/Al_2O_3 model, O* species were dissociated from CO_2 on an interfacial Ru sites (Ru-O-Al) and then easily bridged with the Lewis acid center of Al atoms to form a new Ru-O-Al bond (structure IN1, see Fig. 11), which was an exothermic step with an energy reduction of 0.34 eV (32.8 kJ/mol). The following step was the hydrogenation of an interfacial O atom to form OH* with an energy barrier of 0.31 eV. Then, the further hydrogenation of OH* led to the formation of H_2O with an energy barrier of 0.29 eV. As a consequence, a dynamic incorporation of the interfacial O atom in the bridge Ru-O-Al bond into the final products would easily occur in CO_2 hydrogenation reaction.

The isotope-labeling measurements were carried out on 1% Ru/Al_2O_3 catalyst to clarify the oxygen-exchange process between CO_2 and Ru-O-Al bridge bond. $C^{18}O_2$ gas (^{18}O-95% purity) was used to replace $C^{16}O_2$ under identical reaction conditions and an online mass spectrometer was connected to monitor the mass signals of gaseous products. The isotope-exchange CO_2 reduction reaction started from H_2

introducing (H_2:$C^{18}O_2$= 4:1) when stable signals were reached for the feeding $C^{18}O_2$/He gas. All major gaseous products of both methanation and rWGS in CO_2 hydrogenation were detected on MS spectra, as shown in Fig. 12A. CH_4 and isotopic $C^{18}O$ and $H_2{}^{18}O$, dominated the product distribution, while a small amount of $C^{16}O$ and $H_2{}^{16}O$ have also generated during catalytic reaction, partially due to the co-feeding of $C^{16}O_2$ gas (5%). It should to be emphasized that prominent peaks were emerged on the signal of $H_2{}^{16}O$ (m/z=18) at the initial stage (~5 min) and subsequently equilibrium state was regained. The signal intensity ratio of $H_2{}^{16}O$ (m/z=18) to $H_2{}^{18}O$ (m/z=20) was considerably larger than 5%:95% (the ratio of $C^{16}O_2$:$C^{18}O_2$ in feeding gas) within the first five min, suggesting that ^{18}O-free $H_2{}^{16}O$ was not entirely produced from the hydrogenation reaction of $C^{16}O_2$ impurity with 5% concentration. To further verify the origin of $H_2{}^{16}O$ product, the second reaction run with $C^{18}O_2$ was performed after consecutive treatment of He and H_2/He purgation to remove residual surface species. It was observed that such distinct peak for $H_2{}^{16}O$ (m/z=18) was no longer present in the second run, as shown in Fig. 12B. In addition, similar patterns were obtained on signal channel at m/z 17, which was the main fragment of $H_2{}^{16}O$ that was free from the interferences. These results clearly demonstrated that there were interfacial ^{16}O species on 1% Ru/Al_2O_3 catalyst involving in the exchanging with ^{18}O atoms in $C^{18}O_2$ for producing of $H_2{}^{16}O$ during the initial hydrogenation reaction.

It is reasonably considered that ^{18}O atoms could be left on the interfacial Ru-^{18}O-Al bonds in the spent Ru/Al_2O_3 catalyst after isotopic oxygen-exchange reaction. 18O-free $C^{16}O_2$ hydrogenation reaction was performed over the possibly ^{18}O-labeled 1% Ru/Al_2O_3 catalyst to reveal the role of interfacial bridge oxygen species. When hydrogenation started with sampling of H_2 into $C^{16}O_2$/He gas flow, the signal of $H_2{}^{18}O$ (m/z=20) kept flat for the pristine catalyst, whereas the signal rose a peak immediately for the used catalyst, indicating a substantial yield of $H_2{}^{18}O$ in the $C^{16}O_2$ reduction reaction (Fig. 13A). The expected production of $C^{16}O$ (m/z=28) and CH_4 (m/z=15) was also observed, as shown in Fig. 13B. Furthermore, the MS signals of $C^{18}O$ (m/z=30) and $C^{18}O_2$ (m/z=48) were absent during the reaction, which fully excluded the possibility that the ^{18}O atom of $H_2{}^{18}O$ was originated from gaseous or surface residual $C^{18}O_2$. Based on the above isotope-labeling transient analyses, we expected that $H_2{}^{18}O$ is derived from the incorporation of ^{18}O atoms in interfacial Ru-^{18}O-Al bonds that was produced via the oxygen-exchange process during the first run of $C^{18}O_2$ hydrogenation reaction.

Combined with the isotope-exchange experimental evidences and the theoretic calculation results, CO_2 preferred to be activated and converted into CO on the monolayer Ru sites that directly interacted with the γ-Al_2O_3 support by following the rWGS pathway. Noticeably, the activated dissociation of CO_2 on the monolayer Ru sites left an active O* that further bridges with adjacent Al site of the support to form a ‘new’ interfacial Ru-O-Al bond, achieving the oxygen-exchange between CO_2 and

Ru-Al_2O_3 interface. The illustration of ambient pressure CO_2 hydrogenation reaction catalyzed by Ru/Al_2O_3 catalysts was proposed in Scheme 1.

The rWGS reaction, as the reverse process of water-gas shift, was generally considered as a kind of interfacial structure-sensitive reaction. For instance, the Pt-O_v-Ti^{3+} species formed at the interface between Pt and reducible TiO_2 support was identified as the active sites for the CO formation [64]. According to the analyses of in-situ DRIFTs spectroscopy and microcalorimetry measurements, Pt-O(OH)-K interfaces were evidenced as the primary active sites to achieve CO_2 activation and CO production via bridge-bonded formates intermediates [65]. Similarly, atomically dispersed Rh sites received the directly transferred electrons from the interface with TiO_2 support, favoring the rWGS reaction route in CO_2 hydrogenation, and a strong correlation was obtained between the TOF_{rWGS} value and the fraction of isolated Rh sites [47]. The finding of interfacial oxygen-exchange during the CO_2 activation in this work provides a novel insight into the catalytic effects of the metal-oxide interfaces.

4. Conclusions

In summary, different structure types of Ru sites on γ-Al_2O_3 were prepared via varying the Ru weight loadings and were identified by the comprehensive analyses of H_2-O_2 titration, STEM, EXAFS and CO adsorption IRAS measurements. The monolayer and 3D nanocluster sites of Ru metals are co-existed in 1% Ru/Al_2O_3 catalyst while the latter predominates over 2% and 3% Ru/Al_2O_3 catalysts. By

integrating kinetic measurements and theoretical calculations, the rWGS route to form CO preferentially occurs on monolayer Ru sites, while the methanation route to form CH_4 is in favor of relatively larger 3D Ru nanoclusters. In addition, a dynamic oxygen-exchange process between CO_2 and interfacial Ru-O-Al bond in monolayer Ru-catalyzed rWGS reaction was validated by theoretical calculation results and experimental isotope-labeling studies. The dissociative adsorption of CO_2 at monolayer Ru sites leaves O* species to facilely bridge with the surface Al sites from the γ-Al_2O_3 support, building new interfacial Ru-O-Al bonds via the oxygen-exchange process. The observation in this work highlights the catalytic effects of the active metal-support interfaces in the effective activation of CO_2 for the exploration of the supported metallic catalysts.

Acknowledgments

The authors thank Prof. Hong He and Prof. Yunbo Yu for the help in EXAFS and isotope-exchange analyses. We are grateful for financial support from the Jiangsu Provincial Department of Education and Natural Science Foundation (17KJB150021 and BK20170986). We also thank the support from Campus for Research Excellence and Technological Enterprise (CREATE) program of National Research Foundation (NRF) in Singapore.

References

[1] W. Wang, S. Wang, X. Ma, J. Gong, Recent advances in catalytic hydrogenation of carbon dioxide, Chem. Soc. Rev. 40 (2011) 3703-3727.

[2] M. Aresta, A. Dibenedetto, A. Angelini, Catalysis for the valorization of exhaust carbon: From CO_2 to chemicals, materials, and fuels. Technological use of CO_2, Chem. Rev. 114 (2014) 1709-1742.

[3] M. Behrens, Methanol synthesis over $Cu/ZnO/Al_2O_3$: The active site in industrial catalysis, Science 336 (2012) 893-897.

[4] P. Gao, S. Li, X. Bu, S. Dang, Z. Liu, H. Wang, L. Zhong, M. Qiu, C. Yang, J. Cai, W. Wei, Y. Sun, Direct conversion of CO_2 into liquid fuels with high selectivity over a bifunctional catalyst, Nat. Chem. 9 (2017) 1019-1024.

[5] J. Graciani, K. Mudiyanselage, F. Xu, A.E. Baber, J. Evans, S.D. Senanayake, D.J. Stacchiola, P. Liu, J. Hrbek, J.F. Sanz, J.A. Rodriguez, Highly active copper-ceria and copper-ceria-titania catalysts for methanol synthesis from CO_2, Science 345 (2014) 546-550.

[6] Y. Yan, Y.H. Dai, H. He, Y.B. Yu, Y.H. Yang, A novel W-doped Ni-Mg mixed oxide catalyst for CO_2 methanation, Appl. Catal. B-Environ. 196 (2016) 108-116.

[7] Y. Yan, Y.H. Dai, Y.H. Yang, A.A. Lapkin, Improved stability of Y_2O_3 supported Ni catalysts for CO_2 methanation by precursor-determined metal-support interaction, Appl. Catal. B-Environ. 237 (2018) 504-512.

[8] P. Sabatier, J.B. Senderens, New synthesis of methane, CR Acad. Sci. Paris 134 (1902) 689-691.

[9] X. Wang, H. Shi, J.H. Kwak, J. Szanyi, Mechanism of CO_2 hydrogenation on Pd/Al_2O_3 catalysts: Kinetics and transient DRIFTS-MS studies, ACS Catal. 5 (2015) 6637-6349.

[10] J.N. Park, E.W. Mcfarland, A highly dispersed $Pd\text{-}Mg/SiO_2$ catalyst active for methanation of CO_2, J. Catal. 266 (2009) 92-97.

[11] H.Y. Kim, H.M. Lee, J.N. Park, Bifunctional mechanism of CO_2 methanation on $Pd\text{-}MgO/SiO_2$ catalyst: Independent roles of MgO and Pd on CO_2 methanation, J. Phys. Chem. C 114 (2010) 7128-7131.

[12] J.H. Kwak, L. Kovarik, J. Szanyi, Heterogeneous catalysis on atomically dispersed supported metals: CO_2 reduction on multifunctional Pd catalysts, ACS Catal. 3 (2013) 2094-2100.

[13] W. Zhen, B. Li, G. Lu, J. Ma, Enhancing catalytic activity and stability for CO_2 methanation on $Ni\text{-}Ru/\gamma\text{-}Al_2O_3$ via modulating impregnation sequence and controlling surface active species, RSC Adv. 4 (2014) 16472-16479.

[14] A. Beuls, C. Swalus, M. Jacquemin, G. Heyen, A. Karelovic, P. Ruiz, Methanation of CO_2: Further insight into the mechanism over $Rh/\gamma\text{-}Al_2O_3$ catalyst, Appl. Catal. B-Environ. 113-114 (2012) 2-10.

[15] S. Carenco, C. Sassoye, M. Faustini, P. Eloy, D.P. Debecker, H. Bluhm, M. Salmeron, The active state of supported ruthenium oxide nanoparticles during xarbon sioxide methanation, J. Phys. Chem. C 120 (2016) 15354-15361.

[16] S. Akamaru, T. Shimazaki, M. Kubo, T. Abe, Density functional theory analysis of methanation reaction of CO_2 on Ru nanoparticle supported on TiO_2(101), Appl. Catal. A-Gen. 470 (2014) 405-411.

[17] A.M. Abdel-Mageed, S. Eckle, H.G. Anfang, R.J. Behm, Selective CO methanation in CO_2-rich H_2 atmospheres over a Ru/zeolite catalyst: The influence of catalyst calcination, J. Catal. 298 (2013) 148-160.

[18] F. Wang, S. He, H. Chen, B. Wang, L. Zheng, M. Wei, D.G. Evans, X. Duan, Active site dependent reaction mechanism over Ru/CeO_2 catalyst toward CO_2 methanation, J. Am. Chem. Soc. 138 (2016) 6298-6305.

[19] J. Jia, C. Qian, Y. Dong, Y.F. Li, H. Wang, M. Ghoussoub, K.T. Butler, A. Walsh, G.A. Ozin, Heterogeneous catalytic hydrogenation of CO_2 by metal oxides: defect engineering-perfecting imperfection, Chem. Soc. Rev. 46 (2017) 4631-4644.

[20] W. Wang, S. Wang, X. Ma, J. Gong, Recent advances in catalytic hydrogenation of carbon dioxide, Chem. Soc. Rev. 40 (2011) 3703-3727.

[21] Y.H. Dai, Y. Wang, B. Liu, Y.H. Yang, Metallic nanocatalysis: An accelerating seamless integration with nanotechnology, Small, 11 (2015) 268-289.

[22] F. Wang, C. Li, X. Zhang, M. Wei, D.G. Evans, X. Duan, Catalytic behavior of supported Ru nanoparticles on the {100}, {110}, and {111} facet of CeO_2, J. Catal. 329 (2015) 177-186.

[23] K. Larmier, W.C. Liao, S.H. Tada, E. Lam, R. Verel, A. Bansode, A. Urakawa, A. Comas-Vives, C. Coperet, CO_2-to-methanol hydrogenation on zirconia-supported

copper nanoparticles: Reaction intermediates and the role of the metal-support interface, Angew. Chem. Int. Ed. 56 (2017) 2318-2323.

[24] B. Mutz, M. Belimov, W. Wang, P. Sprenger, M.-A. Serrer, D. Wang, P. Pfeifer, W. Kleist, J.-D. Grunwaldt, Potential of an alumina-supported Ni_3Fe catalyst in the methanation of CO_2: Impact of alloy formation on activity and stability, ACS Catal. 7 (2017) 6802-6814.

[25] M. Cargnello, C.B. Murray, Control of metal nanocrystal size reveals metal-support interface role for ceria catalysts, Science 341 (2013) 771-773.

[26] L.C. Liu, A. Corma, Metal catalysts for heterogeneous catalysis: From single atoms to nanoclusters and nanoparticles, Chem. Rev. 118 (2018) 4981-5079.

[27] G.N. Vayssilov, Y. Lykhach, A. Migani, T. Staudt, G.P. Petrova, N. Tsud, T. Skála, A. Bruix, F. Illas, K.C. Prince, V.r. Matolın, K.M. Neyman, J. Libuda, Support nanostructure boosts oxygen transfer to catalytically active platinum nanoparticles, Nat. Mater. 10 (2011) 310-315.

[28] M.C. Silaghi, A. Comasvives, C. Copéret, CO_2 activation on Ni/γ-Al_2O_3 catalysts by first-principles calculations: From ideal surfaces to supported nanoparticles, ACS Catal. 6 (2016) 4501-4505.

[29] S. Tada, R. Kikuchi, Mechanistic study and catalyst development for selective carbon monoxide methanation, Catal. Sci. Technol. 5 (2015) 3061-3070.

[30] M. Ahmadi, H. Mistry, B. Roldan Cuenya, Tailoring the catalytic properties of metal nanoparticles via support interactions, J. Phys. Chem. Lett. 7 (2016) 3519-3533.

[31] S.J. Tauster, S.C. Fung, R.L. Garten, Strong metal-support interactions. Group 8 noble metals supported on titanium dioxide, J. Am. Chem. Soc. 100 (1978) 170-175.

[32] S.J. Tauster, S.C. Fung, Strong metal-support interactions: Occurrence among the binary oxides of groups IIA-VB, J. Catal. 55 (1978) 29-35.

[33] R. Prins, Hydrogen spillover. Facts and fiction, Chem. Rev. 112 (2012) 2714-2738.

[34] A. Karelovic, P. Ruiz, Improving the hydrogenation function of Pd/γ-Al_2O_3 catalyst by Rh/γ-Al_2O_3 addition in CO_2 methanation at low temperature, ACS Catal. 3 (2013) 2799-2812.

[35] S.W. Li, Y. Xu, Y.F. Chen, W. Z. Li, L.L. Lin, M.Z. Li, Y.C. Deng, Y.C. Deng, X.P. Wang, B.H. Ge, C. Yang, S.Y. Yao, J.L. Xie, Y.W. Li, X. Liu, D. Ma, Tuning the selectivity of catalytic carbon dioxide hydrogenation over iridium/cerium oxide catalysts with a strong metal-support interaction, Angew. Chem. Int. Ed. 56 (2017) 10761-10765.

[36] S.K. Beaumont, S. Alayoglu, C. Specht, W.D. Michalak, V.V. Pushkarev, J. Guo, N. Kruse, G.A. Somorjai, Combining in situ NEXAFS spectroscopy and CO_2 methanation kinetics to study Pt and Co nanoparticle catalysts reveals key insights into the role of platinum in promoted cobalt catalysis, J. Am. Chem. Soc. 136 (2014) 9898-9901.

[37] S. Kattel, W.T. Yu, X.F. Yang, B.H. Yan, Y.Q. Huang, W.M. Wan, P. Liu, J.G. Chen, CO_2 hydrogenation over oxide-supported PtCo catalysts: The role of the oxide support in determining the product selectivity, Angew. Chem. Int. Ed. 55 (2016) 7968-7973.

[38] W. Diao, J.M.M. Tengco, J.R. Regalbuto, J.R. Monnier, Preparation and characterization of Pt-Ru bimetallic catalysts synthesized by electroless deposition methods, ACS Catal. 5 (2015) 5123-5134.

[39] Kresse, Hafner, W. Hauptstrasse, A. Wien, Ab initio molecular dynamics for open-shell transition metals, Pyhs. Rev. B 48 (1993) 13115-13118.

[40] G. Kresse, J. Furthmüller, Efficient iterative schemes for ab initio total-energy calculations using a plane-wave basis set, Pyhs. Rev. B 54 (1996) 11169-11186.

[41] G. Kresse, D. Joubert, From ultrasoft pseudopotentials to the projector augmented-wave method, Pyhs. Rev. B 59 (1999) 1758-1775.

[42] A. Goguet, F.C. Meunier, D. Tibiletti, J.P. Breen, R. Burch, Spectrokinetic investigation of reverse water-gas-shift reaction intermediates over a Pt/CeO_2 catalyst, J. Phys. Chem. B 108 (2004) 20240-20246.

[43] F. Solymosi, A. Erdöhelyi, Hydrogenation of CO_2 to CH_4 over alumina-supported noble metals, J. Mol. Catal. 8 (1980) 471-474.

[44] F. Solymosi, A. Erdöhelyi, T. Bánsági, Methanation of CO_2 on supported rhodium catalyst, J. Catal. 68 (1981) 371-382.

[45] G.D. Weatherbee, C.H. Bartholomew, Hydrogenation of CO_2 on group VIII metals: IV. Specific activities and selectivities of silica-supported Co, Fe, and Ru, J. Catal. 87 (1984) 352-362.

[46] A. Karelovic, P. Ruiz, CO_2 hydrogenation at low temperature over Rh/γ-Al_2O_3 catalysts: Effect of the metal particle size on catalytic performances and reaction mechanism, Appl. Catal. B-Environ. 113-114 (2012) 237-249.

[47] J.C. Matsubu, V.N. Yang, P. Christopher, Isolated metal active site concentration and stability control catalytic CO_2 reduction selectivity, J. Am. Chem. Soc. 137 (2015) 3076-3084.

[48] M. Chen, D. Kumar, C.W. Yi, D.W. Goodman, The promotional effect of gold in catalysis by palladium-gold, Science 310 (2005) 291-293.

[49] J. Shan, M. Li, L.F. Allard, S. Lee, M. Flytzani-Stephanopoulos, Mild oxidation of methane to methanol or acetic acid on supported isolated rhodium catalysts, Nature 551 (2017) 605-608.

[50] J. Aßmann, E. Löffler, A. Birkner, M. Muhler, Ruthenium as oxidation catalyst: bridging the pressure and material gaps between ideal and real systems in heterogeneous catalysis by applying DRIFT spectroscopy and the TAP reactor, Catal. Today 85 (2003) 235-249.

[51] S. Eckle, Y. Denkwitz, R.J. Behm, Activity, selectivity, and adsorbed reaction intermediates/reaction side products in the selective methanation of CO in reformate gases on supported Ru catalysts, J. Catal. 269 (2010) 255-268.

[52] H. Pfnür, D. Menzel, F.M. Hoffmann, A. Ortega, A.M. Bradshaw, High resolution vibrational spectroscopy of CO on Ru(001): The importance of lateral interactions, Surf. Sci. 93 (1980) 431-452.

[53] M.F. Brown, R.D. Gonzalez, An infrared study of the adsorption of carbon monoxide on the reduced and oxidized forms of silica supported ruthenium, J. Phys. Chem. 80 (1976) 1731-1735.

[54] G.H. Yokomizo, C. Louis, A.T. Bell, An infrared study of CO adsorption on reduced and oxidized Ru/SiO_2, J. Catal. 120 (1989) 1-14.

[55] A.M. Abdelmageed, D. Widmann, S.E. Olesen, I. Chorkendorff, J. Biskupek, R.J. Behm, Selective CO methanation on Ru/TiO_2 catalysts: Role and influence of metal-support interactions, ACS Catal. 5 (2015) 6753-6763.

[56] P. Winslow, A.T. Bell, Application of transient response techniques for quantitative determination of adsorbed carbon monoxide and carbon present on the surface of a ruthenium catalyst during Fischer-Tropsch synthesis, J. Catal. 86 (1984) 158-172.

[57] A.M. Karim, V. Prasad, G. Mpourmpakis, W.W. Lonergan, A.I. Frenkel, J.G. Chen, D.G. Vlachos, Correlating particle size and shape of supported $Ru/\gamma\text{-}Al_2O_3$ catalysts with NH_3 decomposition activity, J. Am. Chem. Soc. 131 (2009) 12230-12239.

[58] A.M. Abdel-Mageed, S. Eckle, D. Widmann, R.J. Behm, Water assisted dispersion of Ru nanoparticles: The impact of water on the activity and selectivity of supported Ru catalysts during the selective methanation of CO in CO_2-rich reformate, J. Catal. 335 (2016) 79-94.

[59] X. Wang, Y. Hong, H. Shi, J. Szanyi, Kinetic modeling and transient DRIFTS-MS studies of CO_2 methanation over Ru/Al_2O_3 catalysts, J. Catal. 343 (2016) 185-195.

[60] D.C. Upham, A.R. Derk, S. Sharma, H. Metiu, E.W. Mcfarland, CO_2 methanation by Ru-doped ceria: The role of the oxidation state of the surface, Catal. Sci. Technol. 5 (2015) 1783-1791.

[61] J. Ye, C. Liu, D. Mei, Q. Ge, Active oxygen vacancy site for methanol synthesis from CO_2 hydrogenation on In_2O_3(110): A DFT study, ACS Catal. 3 (2013) 1296-1306.

[62] Y. Yang, M.G. White, P. Liu, Theoretical study of methanol synthesis from CO_2 hydrogenation on metal-doped Cu(111) surfaces, J. Phys. Chem. C 116 (2012) 248-256.

[63] Y. Yang, J. Evans, J.A. Rodriguez, M.G. White, P. Liu, Fundamental studies of methanol synthesis from CO_2 hydrogenation on Cu(111), Cu clusters, and Cu/ZnO(0001), Phys. Chem. Chem. Phys. 12 (2010) 9909-9917.

[64] P.G. Blakeman, E.M. Burkholder, H.Y. Chen, J.E. Collier, J.M. Fedeyko, H. Jobson, R.R. Rajaram, The role of pore size on the thermal stability of zeolite supported Cu SCR catalysts, Catal. Today 231 (2017) 312-318.

[65] X.L. Yang, X. Su, X.D. Chen, H.M. Duan, B.L. Liang, Q.G. Liu, X.Y. Liu,Y.J. Ren, Y.Q. Huang, T. Zhang, Promotion effects of potassium on the activity and selectivity of Pt/zeolite catalysts for reverse water gas shift reaction, Appl. Catal. B-Environ. 216 (2017) 95-105.

Table 1. Structural properties of Ru/Al_2O_3 catalysts based on the results of H_2-O_2 titration and IRAS of CO adsorption measurements.

Ru/Al_2O_3 Catalyst	Dispersion[a] (%)	CN[b]	d[b](nm)	Dispersion[b] (%)	Fraction of surface Ru sites[c]		
					monolayer	periphery	nanocluster
1%	44.5	6.51±0.4	0.94±0.10	71.6±7.6	45.4%	10.0%	44.6%
2%	35.1	7.29±0.4	1.27±0.10	52.7±4.2	6.8%	9.7%	83.5%
3%	32.2	7.43±0.4	1.32±0.10	50.8±4.2	1.1%	8.4%	90.8%

[a]Dispersion of surface Ru particles obtained from H_2-O_2 titrations.

[b]Results from EXAFS analyses. CN: Ru-Ru first shell coordination number; d and dispersion of Ru particles were calculated based on semispherical structure model;

[c]Calculated based on IRAS of CO adsorption.

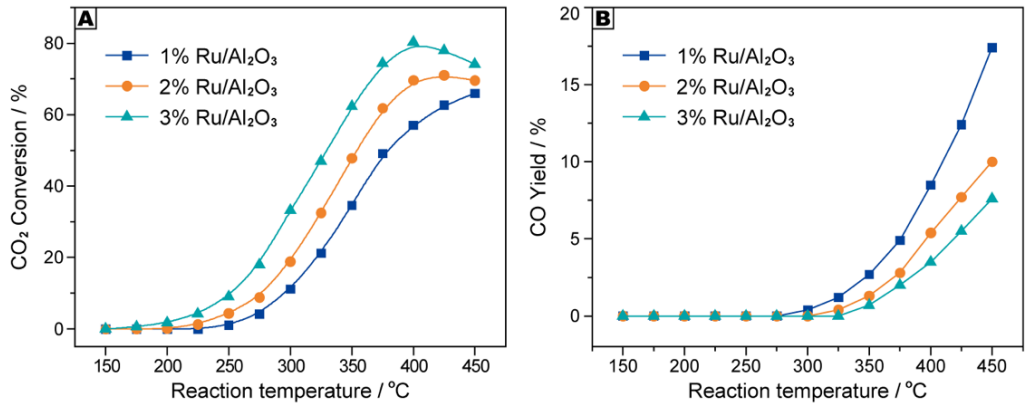

Fig. 1. The catalytic hydrogenation performance (A) CO_2 conversion and (B) CO yield of 1%, 2% and 3% Ru/Al_2O_3 catalysts as a function of reaction temperature.

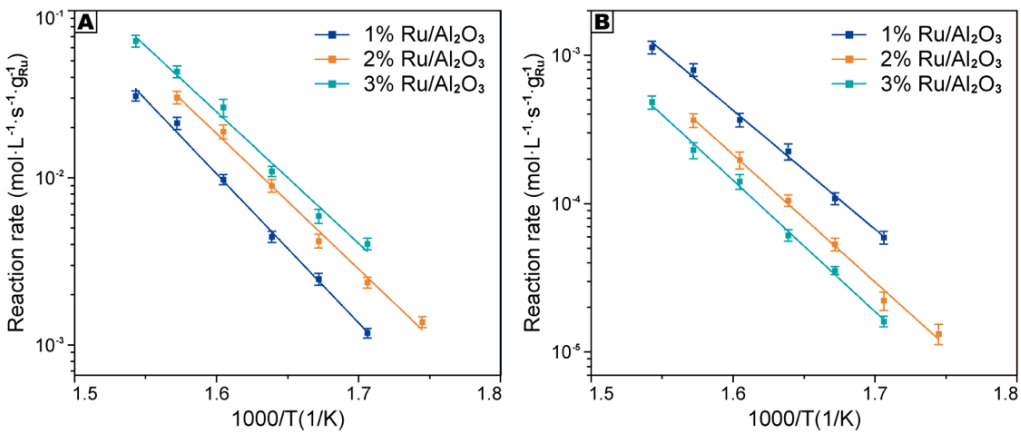

Fig. 2. Arrhenius plots of (A) CH_4 and (B) CO formation rates over Ru/Al_2O_3 catalysts.

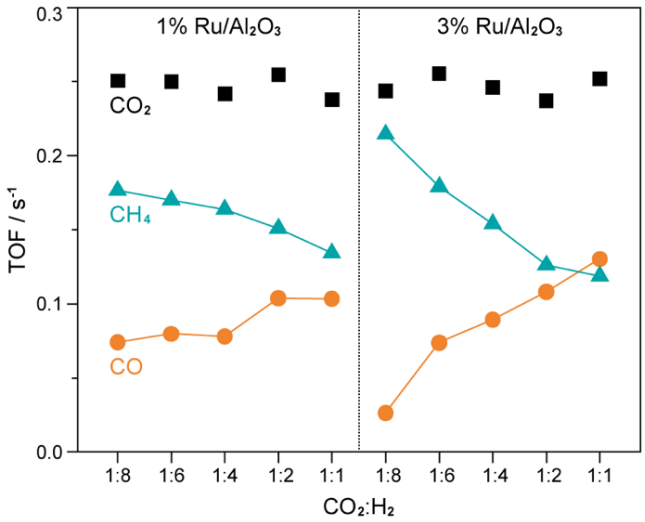

Fig. 3. The TOF for conversion of CO_2, production of CO and CH_4 over 1% and 3% Ru/Al_2O_3 catalysts as a function of CO_2:H_2 ratio.

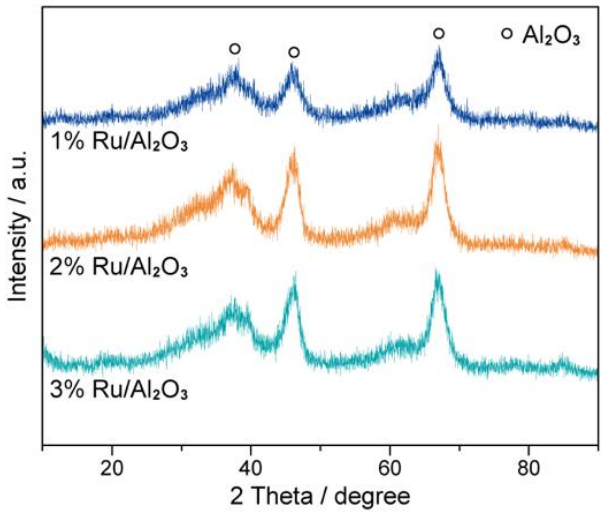

Fig. 4. XRD patterns of Ru/Al_2O_3 catalysts.

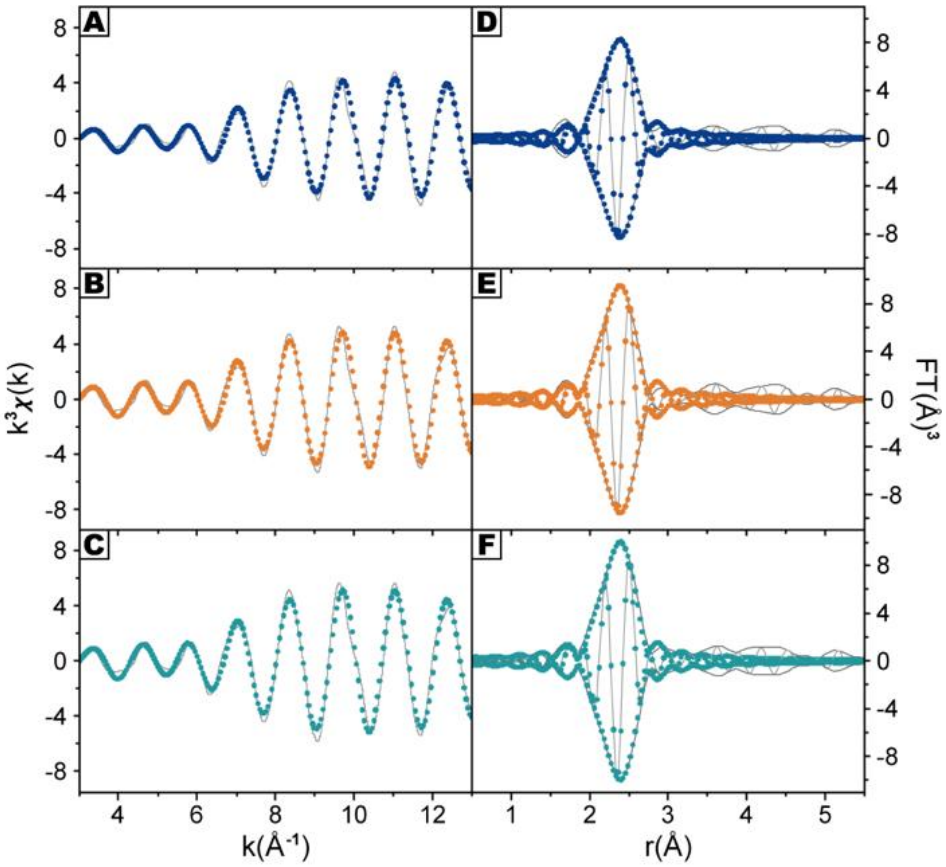

Fig. 5. k^3-weighted χ function and corresponding Fourier transforms obtained on 1% Ru/Al_2O_3 (A and D), 2% Ru/Al_2O_3 (B and E) and 3% Ru/Al_2O_3 (C and F). Solid lines are EXAFS data, and dashed lines are the fits.

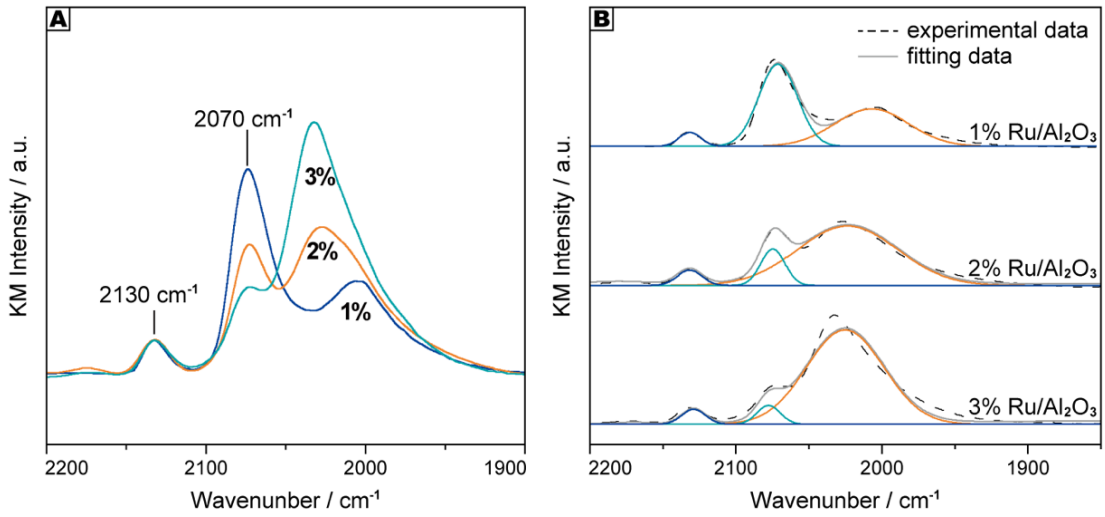

Fig. 6. IRAS spectra for CO adsorption (A) and the deconvoluted data (B) of Ru/Al_2O_3 catalysts.

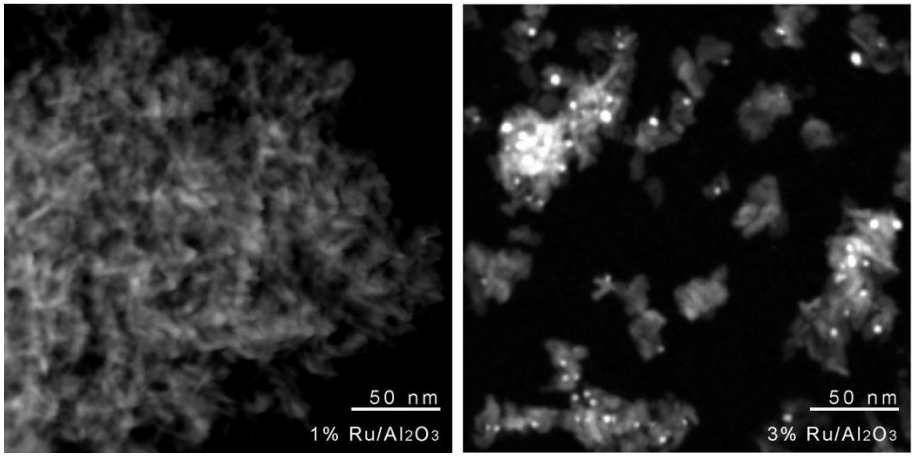

Fig. 7. STEM images of 1% and 3% Ru/Al_2O_3 catalysts.

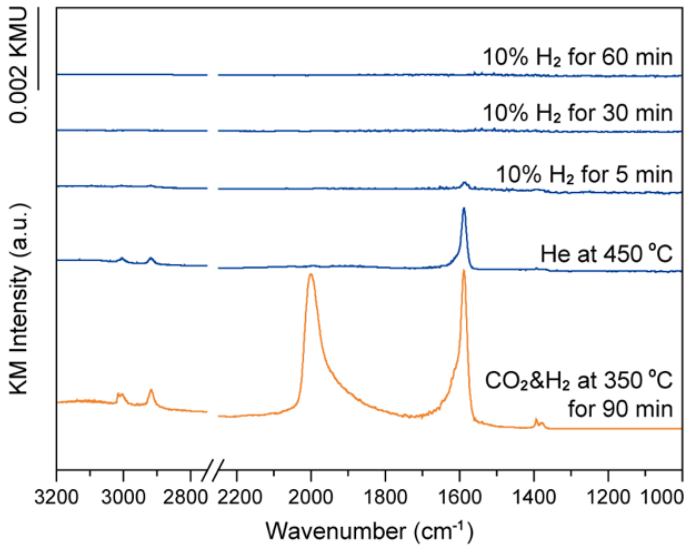

Fig. 8. In-situ DRIFTs spectra collected when the 1% Ru/Al_2O_3 (initially in H_2 and CO_2 flow at 350 ^oC for 90 min) was heated up to 450 ^oC in He at a ramp of 20 ^oC/min, which was then exposed to 10% H_2/He and held there for 5, 30 and 60 min.

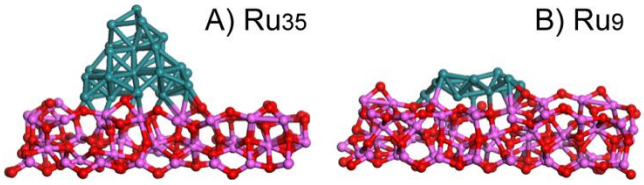

Fig. 9. The optimized model structures of (A) 3D nanocluster Ru_{35}/Al_2O_3 and (B) monolayer Ru_9/Al_2O_3.

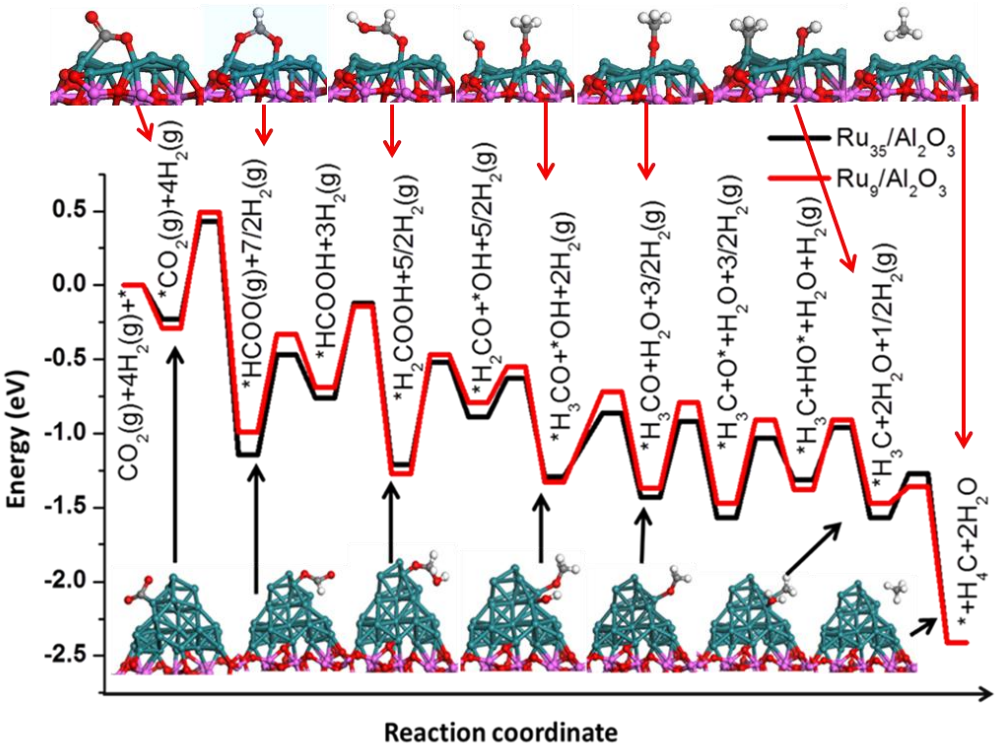

Fig. 10. Potential energy profiles for CO_2 hydrogenation to CH_4 on Ru_{35}/Al_2O_3 and Ru_9/Al_2O_3 models.

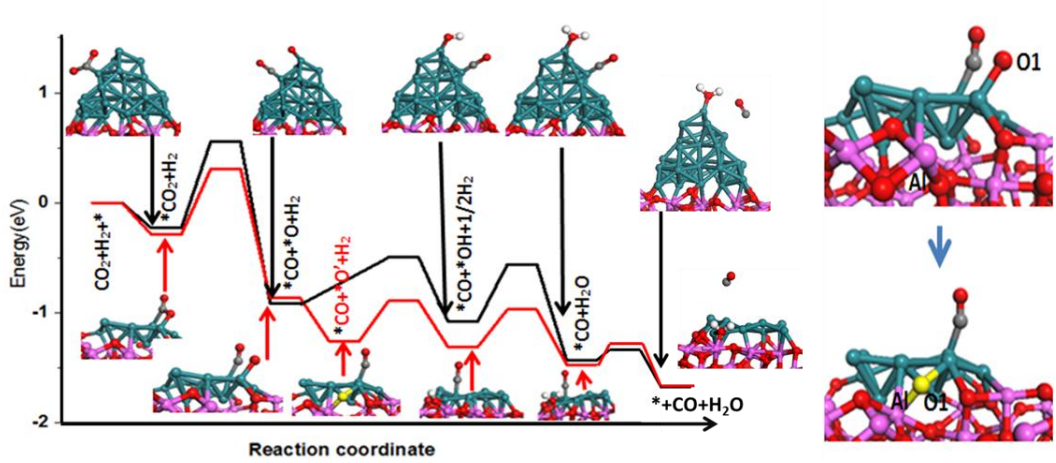

Fig. 11. Potential energy profiles for CO_2 hydrogenation to CO on Ru_{35}/Al_2O_3 and Ru_9/Al_2O_3, along with the structure IN1 (as the right).

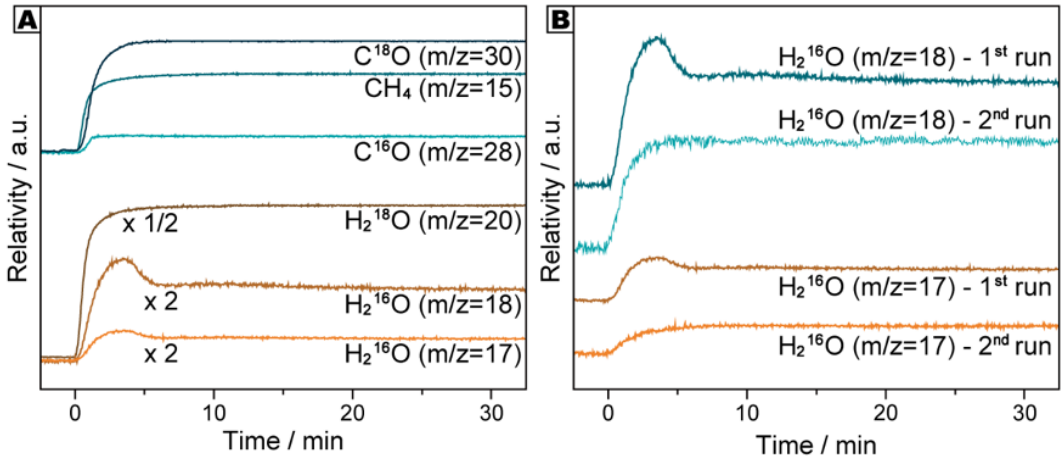

Fig. 12. The MS signals of (A) $H_2{}^{16}O$ (m/z=17, 18) during isotope exposure for two consecutive runs; (B) MS signals in the first run when H_2 was introduced into $C^{18}O_2$/He over pristine 1wt% Ru/Al_2O_3 catalysts.

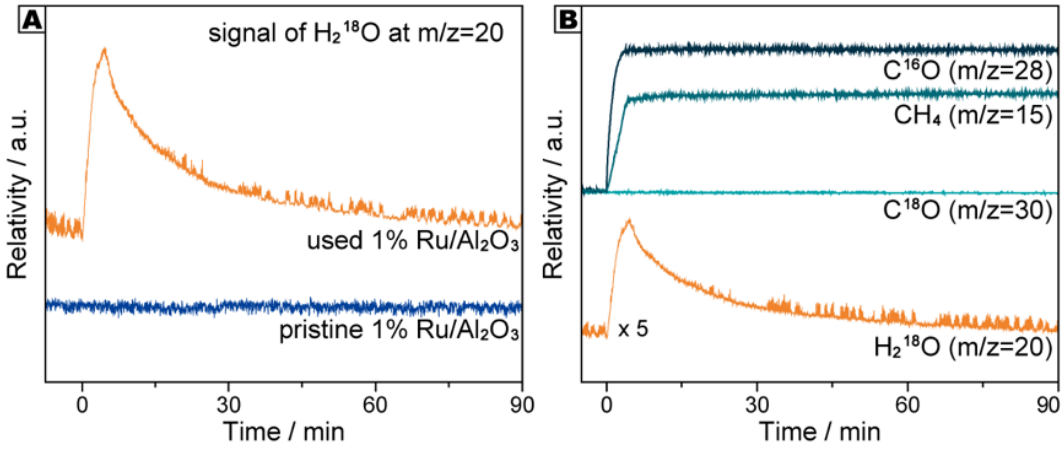

Fig. 13. The MS signals of (A) $H_2{}^{18}O$ (m/z=20) when H_2 was introduced into $C^{16}O_2$/He over used and pristine 1% Ru/Al_2O_3 catalysts; (B) The MS signals as a function of time when H_2 was added into the feed gas of $C^{16}O_2$/He over 1% Ru/Al_2O_3 at 350 ^oC, which is previously exposed to $C^{18}O_2$ and H_2 for 90 min at 350 ^oC.

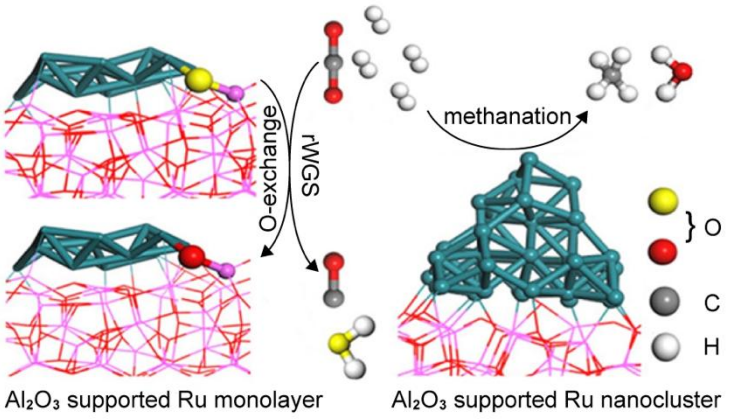

Scheme 1. Schematic illustration of CO_2 hydrogenation to form CO and CH_4 over Ru/Al_2O_3 catalyst.

Graphical Abstract (for review)

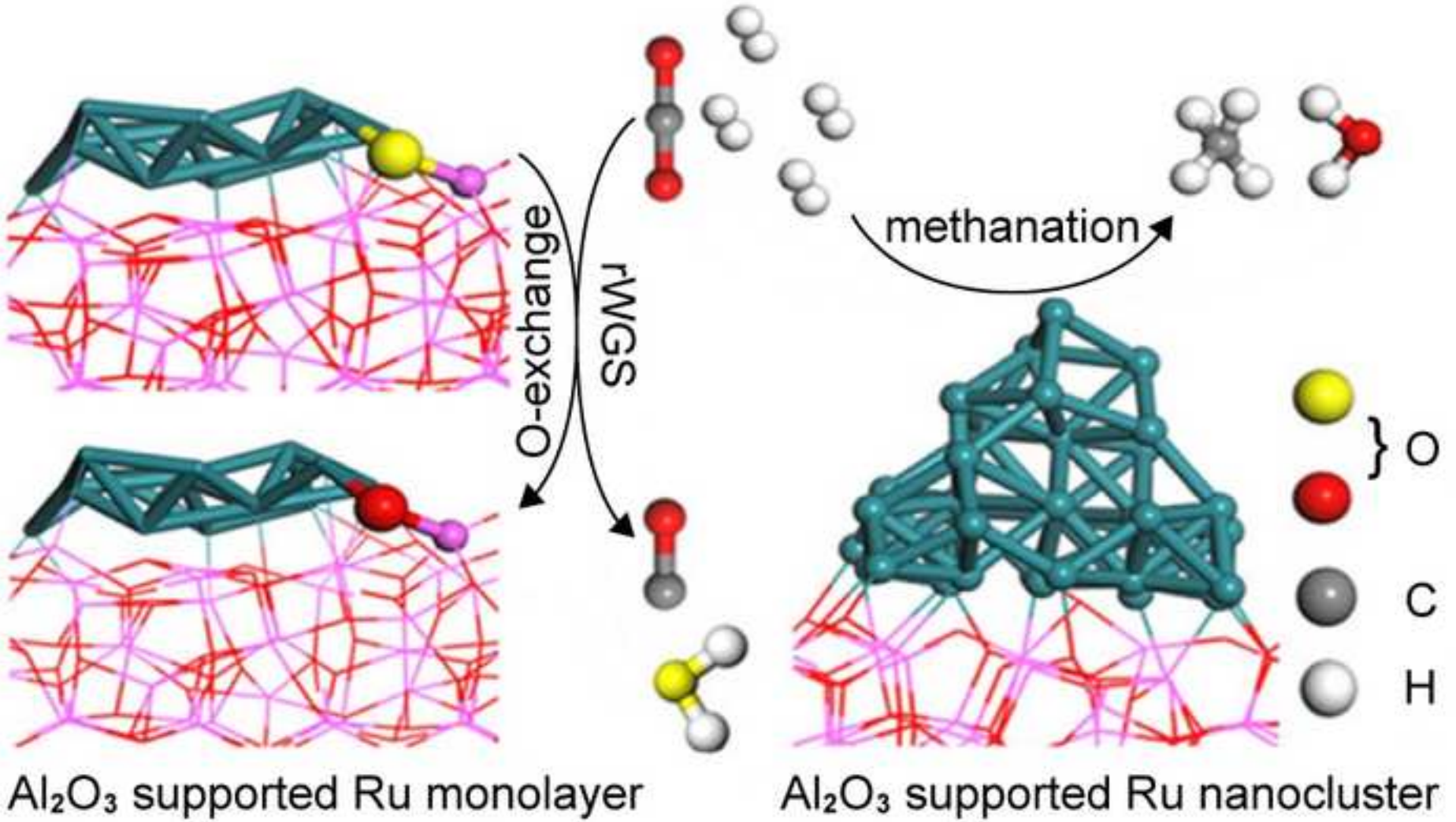

Highlights:

1. Al_2O_3-supported Ru sites determine the selectivity for rWGS and methanation in CO_2 hydrogenation.

2. CO formation prefers monolayer Ru sites while CH_4 formation energetically occurs on relatively larger nanocluster Ru sites.

3. Dynamic oxygen-exchange between O in CO_2 and bridged Ru-O-Al interface is verified for facilitating CO_2 activation.